Cell Reports
Medicine

Article

SARS-CoV-2 infection exacerbates the cellular pathology of Parkinson's disease in human dopaminergic neurons and a mouse model

Graphical abstract

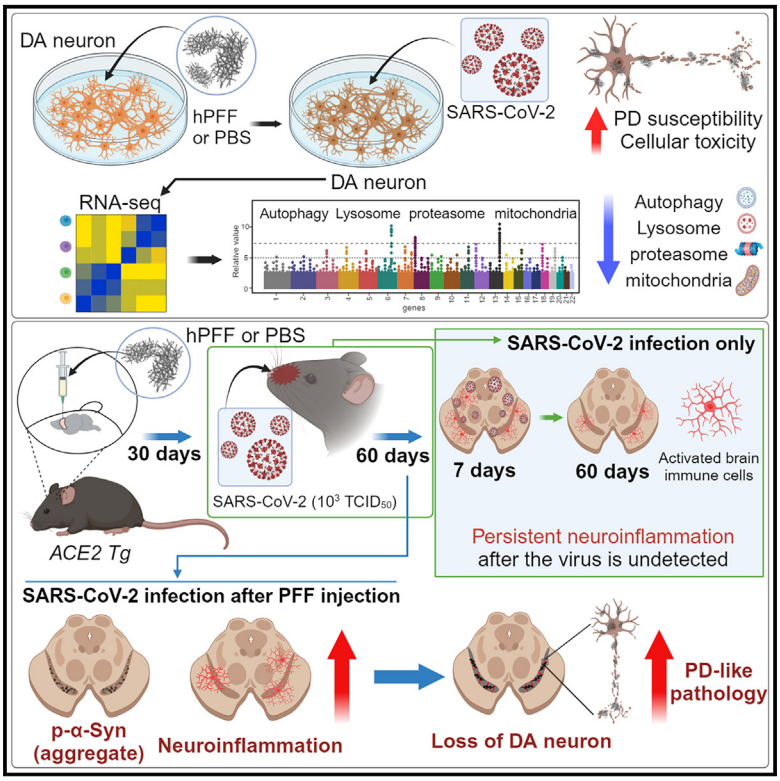

Highlights

- SARS-CoV-2 infection via the nasal cavity spreads to the brain
- Deterioration of Parkinson's disease molecular and cellular phenotype by SARS-CoV-2
- SARS-CoV-2 worsens α-synuclein preformed-fibril-induced dopaminergic neuron death
- SARS-CoV-2 triggers prolonged neuroinflammation for over 60 days in hACE2-Tg mice

Authors

Bina Lee, Ha Nyeoung Choi, Young Hyun Che, ..., Kwang-Soo Lyoo, Yong Jun Kim, Seung Pil Yun

Correspondence

lks1314@wku.ac.kr (K.-S.L.), yjkim1@khu.ac.kr (Y.J.K.), spyun@gnu.ac.kr (S.P.Y.)

In brief

Lee et al. demonstrate that SARS-CoV-2 aggravates neuronal death and neuroinflammation in human embryonic stem cell-derived dopaminergic neurons and a hACE2-Tg mouse model that were both pre-treated with α-synuclein preformed fibrils, highlighting possible long-term neurodegenerative effects of COVID-19 akin to those seen in Parkinson's disease.

Lee et al., 2024, Cell Reports Medicine 5, 101570
May 21, 2024
https://doi.org/10.1016/j.xcrm.2024.101570

CellPress

Cell Reports Medicine

CellPress
OPEN ACCESS

Article

SARS-CoV-2 infection exacerbates the cellular pathology of Parkinson's disease in human dopaminergic neurons and a mouse model

Bina Lee,[1,16] Ha Nyeoung Choi,[1,2,16] Young Hyun Che,[3,4,16] Myungjun Ko,[5,16] Hye Min Seong,[6] Min Gi Jo,[1,4] Seon-Hee Kim,[1] Chieun Song,[6] Subeen Yoon,[3,4] Jiwoo Choi,[3,4] Jeong Hee Kim,[3,4] Minkyeong Kim,[7] Min Young Lee,[8] Sang Won Park,[1,2] Hye Jung Kim,[1,2] Seong Jae Kim,[6] Do Sik Moon,[9] Sun Lee,[4,10] Jae-Hoon Park,[4] Seung-Geun Yeo,[11] Richard G. Everson,[5] Young Jin Kim,[1,2] Kyung-Wook Hong,[12] In-Soon Roh,[13] Kwang-Soo Lyoo,[14,*] Yong Jun Kim,[3,4,10,15,17,*] and Seung Pil Yun[1,2,*]

[1]Department of Pharmacology, Institute of Health Sciences, College of Medicine, Gyeongsang National University, Jinju 52727, Republic of Korea
[2]Department of Convergence Medical Science, College of Medicine, Gyeongsang National University, Jinju 52727, Republic of Korea
[3]Department of Biomedical Science, Graduate School, Kyung Hee University, Seoul 02447, Republic of Korea
[4]Department of Pathology, College of Medicine, Kyung Hee University, Seoul 02447, Republic of Korea
[5]Department of Neurosurgery, David Geffen School of Medicine, University of California, Los Angeles, Los Angeles, CA 90095, USA
[6]Department of Ophthalmology, Institute of Health Sciences, College of Medicine, Gyeongsang National University, Jinju 52727, Republic of Korea
[7]Department of Neurology, Gyeongsang National University Hospital, Jinju 52727, Republic of Korea
[8]College of Pharmacy, Research Institute of Pharmaceutical Sciences, BK21 FOUR ERGID, Vessel-Organ Interaction Research Center (MRC), Kyungpook National University, Daegu 4156, Republic of Korea
[9]Department of Pulmonology and Critical Care Medicine, Chosun University Hospital, Gwangju 61453, Republic of Korea
[10]Research Center, TissueIn, Inc., Seoul 06158, Republic of Korea
[11]Department of Otorhinolaryngology - Head and Neck Surgery, School of Medicine, Kyung Hee University, Seoul 02447, Republic of Korea
[12]Division of Infectious Diseases, Department of Internal Medicine, Gyeongsang National University Hospital, Gyeongsang National University College of Medicine, Jinju, Republic of Korea
[13]Division of Foreign Animal Disease, Animal and Plant Quarantine Agency, Gimcheon-si, Gyeongsangbuk-do 39660, Republic of Korea
[14]Department of Veterinary Nursing, College of Health Sciences, Wonkwang University, Iksan 54538, Republic of Korea
[15]KHU-KIST Department of Converging Science and Technology, Kyung Hee University, Seoul 02447, Republic of Korea
[16]These authors contributed equally
[17]Lead contact
*Correspondence: lks1314@wku.ac.kr (K.-S.L.), yjkim1@khu.ac.kr (Y.J.K.), spyun@gnu.ac.kr (S.P.Y.)
https://doi.org/10.1016/j.xcrm.2024.101570

SUMMARY

While an association between Parkinson's disease (PD) and viral infections has been recognized, the impact of severe acute respiratory syndrome coronavirus 2 (SARS-CoV-2) on PD progression remains unclear. Here, we demonstrate that SARS-CoV-2 infection heightens the risk of PD using human embryonic stem cell (hESC)-derived dopaminergic (DA) neurons and a human angiotensin-converting enzyme 2 (hACE2) transgenic (Tg) mouse model. Our findings reveal that SARS-CoV-2 infection exacerbates PD susceptibility and cellular toxicity in DA neurons pre-treated with human preformed fibrils (hPFFs). Additionally, nasally delivered SARS-CoV-2 infects DA neurons in hACE2 Tg mice, aggravating the damage initiated by hPFFs. Mice infected with SARS-CoV-2 display persisting neuroinflammation even after the virus is no longer detectable in the brain. A comprehensive analysis suggests that the inflammatory response mediated by astrocytes and microglia could contribute to increased PD susceptibility associated with SARS-CoV-2. These findings advance our understanding of the potential long-term effects of SARS-CoV-2 infection on the progression of PD.

INTRODUCTION

Amid the coronavirus disease 2019 (COVID-19) pandemic, the global scientific community accomplished an unprecedented milestone by rapidly developing effective vaccines and therapeutics against severe acute respiratory syndrome coronavirus-2 (SARS-CoV-2).[1] As the number of severe cases declines, it becomes imperative to anticipate and mitigate potential long-term consequences in individuals who have recovered from SARS-CoV-2 infection. Notably, a range of manifestations have been documented as sequelae thus far, including encephalitis,[2–5] memory loss,[6] headache (dizziness, nausea),[7] anosmia, and ageusia.[8]

Of particular interest, patients infected with SARS-CoV-2 have exhibited neurological symptoms such as headache, paresthesia, anosmia, dyslexia, ataxia, and alterations in mental status.[2–8] Additionally, the early stages of SARS-CoV-2 infection have been associated with transient structural abnormalities in the brain,[9] neuroinflammatory events,[2–5] and sensory loss such as anosmia.[8] Recent cases have reported the emergence of Parkinsonism in COVID-19 patients either during or shortly after SARS-CoV-2 infection, presenting symptoms such as rigidity, resting tremor in the upper extremities, and bradykinesia.[10] Furthermore, SARS-CoV-2 particles have been detected in the postmortem human cerebrum, midbrain, and cerebrospinal fluid.[11] These findings raise intriguing questions about the potential for SARS-CoV-2 infection in the brain to cause clinically important long-term neurological sequelae.

In a prospective study, Sulzer et al. discussed the brain immune response elicited by SARS-CoV-2 infection,[12] which is characterized by an initial cytokine storm followed by the activation of innate and adaptive immune responses.[13] Importantly, the cytokine storm associated with SARS-CoV-2 infection can trigger microglial activation, which is known to contribute to the pathophysiology of Parkinson's disease (PD).[14] The neuroinflammatory response observed in the development and progression of PD leads to dysfunctions in autophagy within dopaminergic (DA) neurons, endoplasmic reticulum stress, compromised proteostasis, mitochondrial dysfunction, and eventual protein misfolding and aggregation. Recent studies have also suggested that such inflammatory responses could potentially trigger the onset of PD.[15,16]

A recent meta-analysis demonstrated an association between viral infections such as *Helicobacter pylori*, hepatitis C virus, Malassezia, and pneumonia and an increased risk of PD.[17] Interestingly, individuals who have recovered from childhood measles virus infection may also experience the onset of neurodegenerative diseases 10–20 years later.[18,19] In addition, it has been reported that SARS-CoV-2 can infect DA neurons in the human brain, so there is a possibility that it can cause functional changes in neuronal activity.[20–22] Therefore, we hypothesize that SARS-CoV-2 infection within DA neurons, or the concurrent inflammatory response, may persist even after symptomatic recovery, subsequently increasing the risk of PD, particularly in elderly individuals with preexisting risk factors.

The objective of this study was to investigate the potential association between SARS-CoV-2 infection and PD as a long-term consequence. To explore the temporal aspect of the neuroinflammatory effects initiated by SARS-CoV-2 on PD progression, we utilized established human angiotensin-converting enzyme 2 (hACE2) transgenic (Tg) mouse models and human embryonic stem cell (hESC)-derived DA neurons. The results of our investigation demonstrate that SARS-CoV-2 infection promotes the onset of PD by inducing persistent neuroinflammation in microglia and astrocytes, as well as exacerbating direct cytotoxicity in DA neurons triggered by human preformed fibrils (hPFFs). Notably, the neuroinflammatory response persists even after SARS-CoV-2 clearance in the brain, reaching a technically undetectable viral load. This study provides experimental evidence investigating the temporal aspect of the neuroinflammatory effects initiated by SARS-CoV-2 in the context of PD pathogenesis. These findings provide important insights for the identification and prediction of long-term neurological sequelae following SARS-CoV-2 infection and for the appropriate clinical management of survivors.

RESULTS

hPFF-induced PD progression in hDA neurons is increased by direct SARS-CoV-2 infection

Upon differentiation of hESCs according to the protocol, we observed effective expression of neuronal markers in DA neurons (Figures S1A–S1C). Additionally, we verified the quality of the hPFFs used in the experiments, confirming successful aggregation and cleavage to a size suitable for cellular uptake (Figures S1D–S1I). The length of sonicated hPFFs was measured using transmission electron microscopy images and ImageJ software. Our data revealed that more than 75% of the total fibers were PFFs with a length of less than 50 nm (Figure S1G). Shorter fibers have been shown to enhance seed picking efficiency, and the optimal length of PFFs appears to be around 50 nm.[23,24]

To determine the appropriate MOI without cytotoxicity, DA neurons were treated with viruses ranging from 0.1 to 1.0 MOI. The expression of the nucleocapsid protein (NP) (SARS-CoV-2 marker) protein exhibited an MOI-dependent increase (Figures S2A and S2B), while the TH protein level decreased (Figures S2A and S2C), meaning there was a higher incidence of DA neuronal injury (Figure S2D) at 1.0 MOI. The validation of hACE2, TH, and α-synuclein (α-Syn) expression was conducted in hDA neurons (Figure S2E). Direct infection of human dopaminergic (hDA) neurons with SARS-CoV-2 at an MOI of 0.1 using the Allplex SARS-CoV-2 Assay Kit (Seegene, Seoul Korea), designed for clinical detection of SARS-CoV-2 in Korea, confirmed infection (Figure S2F). A lower threshold cycles (CT) value served as evidence of SARS-CoV-2 infection. Additionally, significant alterations in SARS-CoV-2-related genes (nucleocapsid, RNA-dependent RNA polymerase [RdRP], spike) were observed in SARS-CoV-2-infected hDA neurons (Figures S2G–S2L). Importantly, the presence or absence of hPFF treatment in SARS-CoV-2-infected hDA neurons had no impact on SARS-CoV-2 gene expression. Based on these findings, hDA neurons were treated with hPFFs and then infected with the virus at an MOI of 0.1 to observe the PD-like pathology, virus replication, and related proteins (Figure 1A). TH expression was downregulated with hPFF treatment, an effect further accelerated by SARS-CoV-2 infection (Figures 1B and 1C). In the soluble fraction, no difference in α-Syn levels was noted, and phospho-α-Syn (p-α-Syn) was undetected (Figures 1D and 1E). In the insoluble fraction, both p-α-Syn and α-Syn levels increased after hPFF treatment. Notably, when hPFF treatment was combined with SARS-CoV-2 infection, the increase was more pronounced compared to hPFF treatment alone (refer to Figures 1D and 1F). The rise in phosphorylation of α-Syn triggered by SARS-CoV-2 infection following hPFF treatment was further confirmed through confocal microscopy (Figures 1G–1K). Finally, TUNEL and Alamar blue assays demonstrated that SARS-CoV-2 infection, following hPFF treatment, exacerbated apoptosis in hDA neurons (Figures 1L–1N). These results suggest that

CellPress
OPEN ACCESS

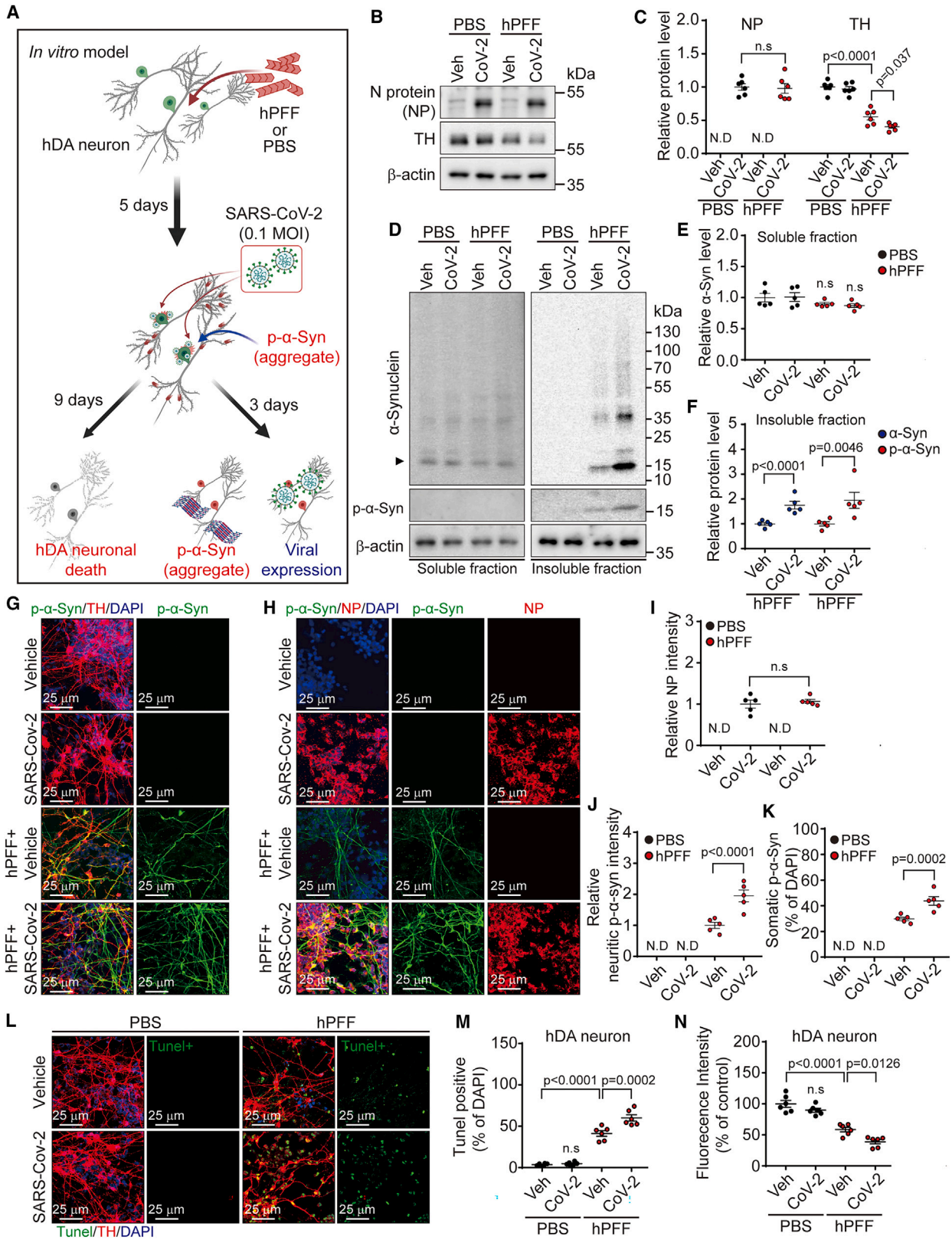

(legend on next page)

SARS-CoV-2 infection exacerbates the pathology caused by hPFF treatment by directly infecting hDA neurons, which was not observed in the condition infected with SARS-CoV-2 alone, as compared to the vehicle control. Treatment of monomeric α-Syn did not affect the expression of p-α-Syn and NP (Figures S3A–S3D). Furthermore, the treatment did not lead to the death of hDA neurons (Figures S3G–S3I), and there was no elevation in susceptibility to PD-like pathology induced by SARS-CoV-2 (Figure S3).

SARS-CoV-2 infection upregulates molecular features associated with PD progression induced by hPFFs

To investigate the influence of SARS-CoV-2 infection on the development of hPFF pathology in hDA neurons, we examined changes in gene expression profiles. Treating DA neurons with hPFFs followed by SARS-CoV-2 infection resulted in increased expression levels in 2,877 genes in hDA neurons (Figure 2A). Ontology analysis showed that the upregulated genes were relevant to neurological diseases such as amyotrophic lateral sclerosis (ALS), parkinsonism, mental retardation, and neurodegeneration (Figure 2B). KEGG pathway analysis revealed changes in the molecular mechanisms linked to neurological diseases including PD, ALS, neurodegeneration, Huntington's disease, and Alzheimer's disease (Figure 2C). Additionally, SARS-CoV-2 infection amplified the increase in the expression of 1,017 genes that were altered by hPFFs and enhanced the decrease in 583 genes (Figure 2D). Pathway analysis with genes involved in hPFF pathology aggravated by SARS-CoV-2 indicated an increase in cell death (apoptosis, autophagy, and mitophagy) and neurodegenerative diseases (PD, Huntington's, neurodegeneration, ALS) and a decrease in DA neuronal synapse (synaptic vesicle cycle, DA neuronal synapse, neurotrophin signaling pathway) (Figure 2E; Tables S1 and S2). Genetic analysis results were further validated using quantitative real-time PCR (real-time qPCR) by categories of biological process in which each gene participates. Apoptosis-related genes such as *FADD*, *BAX*, *BID*, and *CASP9*,[25] as well as autophagy-associating genes such as *WDR45*, *TECPR2*, *MAP1LC3A*, and *SQSTM1*,[26–29] were upregulated in hDA neurons by hPFF treatment alone (Figures 2F and 2G), and a further amplification of the increased level was observed with SARS-CoV-2 infection. Additionally, genes involved in the pathogenesis of PD induced by hPFFs in hDA neurons were validated. The sets of genes that were further altered due to SARS-CoV-2 infection in comparison to hPFF treatment only are involved in the following cellular and molecular processes: oxidative stress (*CYC1* and *COX7b*), adenosine 3′,5′-cyclic monophosphate (*PRKACA* and *PRKAC*), protein aggregation and clearing (*HAP1* and *WDR24*), familial inheritance of PD (*PINK1* and *PPP2CA*), and normal function of DA neurons (*TH* and *KIF5C*) (Figures 2H and 2I).[30–34]

To analyze functional and mechanistic changes, along with RNA alterations, additional experiments were conducted. The expression of LC3A/B and SQSTM1/P62, related to autophagy function, was further reduced in the SARS-CoV-2-infected group after hPFF treatment compared to the hPFF-treated group (Figures 2J and 2K). Also, the expression levels of proteins associated with mitochondrial functions, including succinate dehydrogenase, prohibitin 1, cytochrome *c* oxidase IV, cytochrome *c*, and HSP60, were significantly diminished by hPFF treatment. This diminution was further heightened in the presence of SARS-CoV-2 infection following hPFF treatment (Figures 2L–2O). Furthermore, lysosome and proteasome activities, crucial for the removal of abnormal proteins in the cell, were decreased by hPFF treatment, with a further reduction observed in the SARS-CoV-2-infected group following hPFF treatment (Figures 2P–2R). These data demonstrate that SARS-CoV-2 infection not only significantly alters the expression of genes involved in PD progression induced by PFF treatment but also induces intracellular dysfunction in DA neurons.

SARS-CoV-2 infection in the brain

The tissue culture infective dose 50% ($TCID_{50}$) for SARS-CoV-2 expression in the brain was determined by injecting SARS-CoV-2 at concentrations of 10^3, 10^4, 10^5, and 10^6 $TCID_{50}$ into the nares of hACE2 Tg mice. In the case of 10^5 and 10^6 units of SARS-CoV-2, mice succumbed to the infection on day 7 post-infection, and all mice died on day 10 post-infection (data not shown). In the case of 10^4 MOI infection, two mice died on day 10 post-infection (data not shown). On days 3 and 10, it was confirmed that 10^3 $TCID_{50}$ SARS-CoV-2 infected the whole brain, including the olfactory bulb, striatum (STR), ventral midbrain (VM), hippocampus, cerebrum, and brain stem

Figure 1. Pathology of SARS-CoV-2 infection with hPFF-induced PD in hESC-derived DA neurons

(A) Schematic experimental summary of DA neurons infected with SARS-CoV-2 (0.1 MOI) infection and treated with hPFFs.
(B) Representative western blot bands of nucleocapsid protein (NP) and TH levels in hDA neurons infected with SARS-CoV-2 and then treated with hPFFs.
(C) Quantification of NP and TH levels. $n = 6$, biological repeat.
(D) Representative western blot expression of α-Syn and p-α-Syn in hDA neurons treated with SARS-CoV-2 and/or hPFFs.
(E) Quantification of α-Syn western blot levels. $n = 5$, biological repeat.
(F) Quantification of p-α-Syn western blot levels. $n = 5$, biological repeat, values are mean ± SEM, one-way ANOVA.
(G) Representative immunofluorescence image of p-α-Syn (green) and TH (red).
(H) Representative immunofluorescence image of p-α-Syn (green) and NP (red).
(I) Quantification of NP. $n = 5$, biological repeat, values are mean ± SEM, unpaired two-tailed Student's t tests.
(J) The neuritic p-α-Syn intensity. The intensity excluding the somatic region of p-α-Syn was measured using ImageJ. $n = 5$, biological repeat.
(K) The percentage of somatic p-α-Syn contrasted with DAPI. For the somatic p-α-Syn-positive cells, manual counting was conducted, considering only cells positive for both DAPI and p-α-Syn staining. $n = 5$, biological repeat.
(L) Representative image of TUNEL staining of DA neurons infected with SARS-CoV-2 and treated with hPFFs.
(M) Quantification of TUNEL-positive DA neuron cells. $n = 6$, biological repeat.
(N) A graph showing the difference in cell viability measured with Alamar Blue. $n = 6$, biological repeat, values are mean ± SEM, one-way ANOVA.
n.s., non-significance; N.D., non-detection.
See also Figures S1–S3.

CellPress
OPEN ACCESS

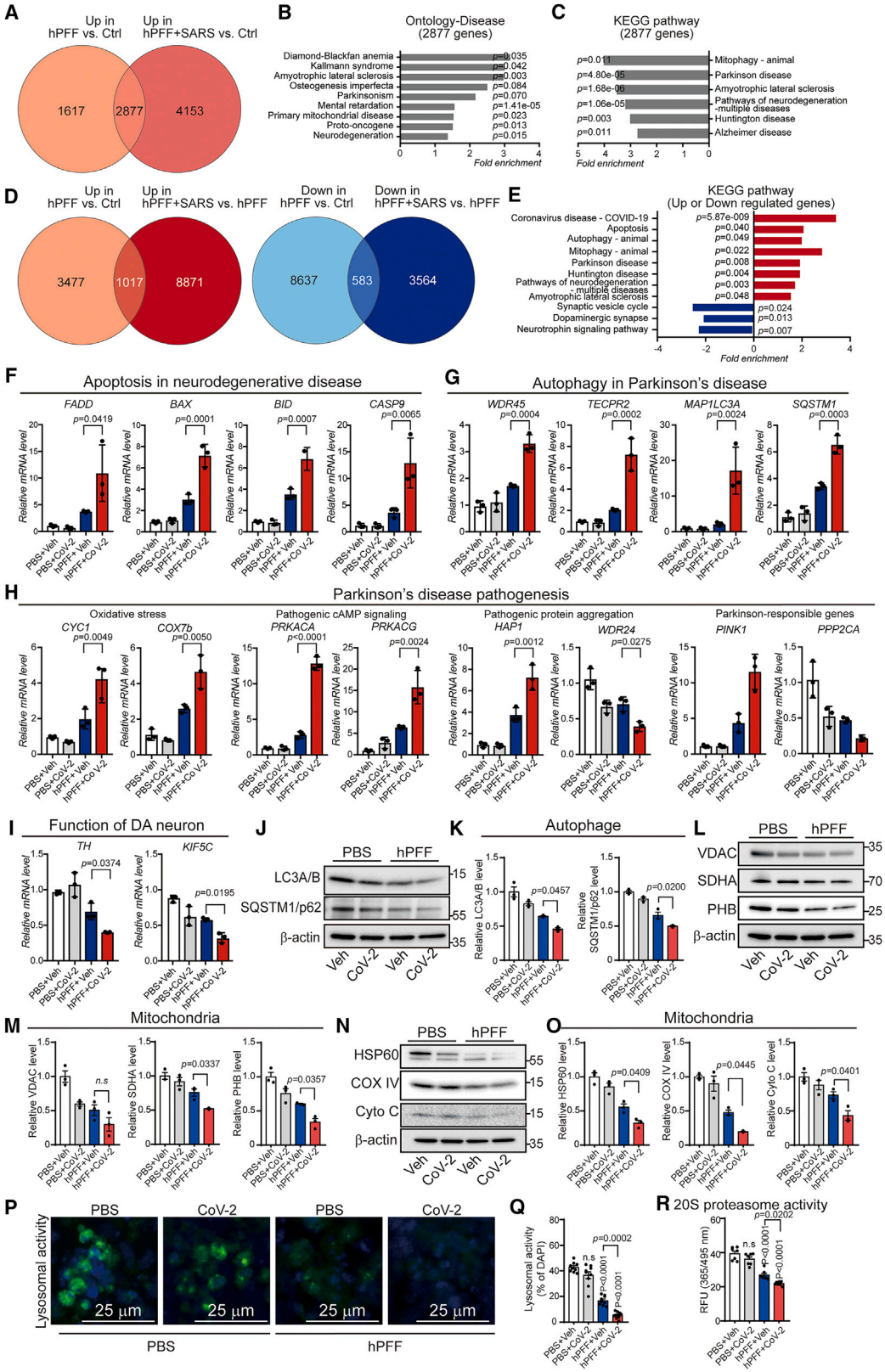

(legend on next page)

(Figures 3A–3D). There was a significant increase in NP expression levels at day 10 compared to day 3 across the brain (Figure 3E). These results suggested that SARS-CoV-2 infection through intranasal injection can spread to the central nervous system. Finally, based on this titration experiment result, 10^3 $TCID_{50}$ SARS-CoV-2 was utilized for the subsequent *in vivo* experiment.

SARS-CoV-2 increased hPFF-induced PD-like pathology

To verify the potential contribution of SARS-CoV-2 infection to the early onset of PD, we injected hPFFs or vehicle into the STR of ACE2 Tg mice, followed by 10^3 $TCID_{50}$ SARS-CoV-2 infection 30 days later (Figure 4A). After 60 days, sacrificed mice were analyzed for PD-like pathology (Figure 4A). SARS-CoV-2 (NP) was detected 7 days post-infection in the brain but not 60 days post-infection in the substantia nigra pars compacta (SNpc) of the VM (Figures 4B and 4C). In mice of the hPFF with SARS-CoV-2 infection group, phosphorylation of α-Syn induced by hPFF treatment significantly increased compared to the hPFF-only group (Figure 4E). We subsequently quantified the intensity of the TH signal in the group that was infected with SARS-CoV-2 in addition to hPFF treatment, which was significantly lower than that in the group treated solely with hPFFs (Figure 4H). Furthermore, in the VM and STR of SARS-CoV-2-infected mice treated with hPFFs, the expression levels of the TH and dopamine transporter (DAT) proteins were significantly lower than those in uninfected mice treated with hPFFs alone, while the α-Syn level was comparable (Figures 4H, 4I, and S4). Despite not causing the loss of TH-positive cells until 60 days after virus clearance, assuming the presence of pathological factors capable of triggering PD, SARS-CoV-2 has the potential to induce the loss of TH-positive cells.

SARS-CoV-2 infection influences neuroinflammation

Activation of GFAP (astrocyte marker, Figures 5A, 5B, 5E, and 5F) and Iba-1 (microglia marker, Figures 5C–5F) persisted for up to 60 days post-infection, even only with SARS-CoV-2 infection. At the 60-day time point, SARS-CoV-2 infection without hPFFs did not induce DA neuronal loss in the immunohistochemistry (IHC) staining for TH in the substantia nigra of the VM (Figures 5G and 5H). Western blot analysis of the VM from mice infected with SARS-CoV-2 showed no changes in TH, DAT, or α-Syn protein expression (Figures 5I and 5J). These data strongly suggested that SARS-CoV-2 infection initially induce neuroinflammation in the brain, which persists for an extended period. While the SARS-CoV-2 virus alone did not cause neurological damage until 60 days after viral particles became undetectable, it is likely to be a risk factor for the exacerbation of PD pathological symptoms when there is an underlying risk factor, as represented in this study by hPFFs. Although the study is limited to validating the direct infection of brain glial cells, such as astrocyte and microglia with SARS-CoV-2, the co-localization of brain glial cells with the SARS-CoV-2 marker NP in the same region has been confirmed (Figure S5).

To compare the effects of different SARS-CoV-2 variants (wild-type SARS-CoV-2 [$SARS\text{-}CoV\text{-}2^{WT}$] and delta-variant SARS-CoV-2 [$SARS\text{-}CoV\text{-}2^{delta}$]) on the brain, we infected mice with the same 10^3 $TCID_{50}$ of $SARS\text{-}CoV\text{-}2^{WT}$ and $SARS\text{-}CoV\text{-}2^{delta}$ for 7 days. $SARS\text{-}CoV\text{-}2^{delta}$ infects the SNpc of the VM, resembling the pattern of $SARS\text{-}CoV\text{-}2^{WT}$ (Figures S6A–S6C). Western blot results showed comparable TH and DAT expression levels, but the NP expression level was slightly higher with $SARS\text{-}CoV\text{-}2^{delta}$ infection (Figures S6D and F6E). $SARS\text{-}CoV\text{-}2^{delta}$ also upregulated the expression of GFAP and Iba-1 (Figures S6F–S6K). However, the difference in the expression levels of GFAP and Iba-1 between $SARS\text{-}CoV\text{-}2^{WT}$ and $SARS\text{-}CoV\text{-}2^{delta}$ was not statistically significant. These results indicate that despite the slightly higher infection capacity of $SARS\text{-}CoV\text{-}2^{delta}$ compared to $SARS\text{-}CoV\text{-}2^{WT}$, SARS-CoV-2 infection induces neuroinflammation regardless of delta variation.

Figure 2. Molecular pathogenesis of SARS-CoV-2 infection with hPFF-induced PD progression in hESC-derived DA neurons

(A) Venn diagram indicating upregulated genes related to hPFF-induced PD progression or hPFF-induced PD progression with SARS-CoV-2 (0.1 MOI) infection.
(B) Results of Gene Ontology analysis using genes upregulated in hPFF-induced PD progression and hPFF-induced PD progression with SARS-CoV-2 infection.
(C) Results of KEGG pathway analysis using genes upregulated in hPFF-induced PD progression and hPFF-induced PD progression with SARS-CoV-2 infection.
(D) Venn diagram illustrating genes involved in the pathogenesis of hPFF-induced PD progression that are exacerbated by SARS-CoV-2 infection.
(E) The results of KEGG pathway analysis employing genes that are exacerbated by SARS-CoV-2 infection among genes involved in hPFF-induced PD progression.
(F) Validation of neuronal-apoptosis-related gene expression using quantitative real-time PCR. $n = 3$, biological replicates.
(G) Validation of PD-associating autophagy-related gene expression using quantitative real-time PCR. $n = 3$, biological repeat.
(H) Validation of PD pathogenesis-associated gene expression using quantitative real-time PCR $n = 3$, biological repeat.
(I) Validation of DA neuron functional gene expression levels using quantitative real-time PCR. $n = 3$, biological repeat, values are mean ± SD, one-way ANOVA.
(J) Representative western blot images of LC3A/B and SQSTM1/p62 to analyze autophagic function in human DA neurons.
(K) Quantitative graphs of LC3A/B and SQSTM1/p62 from (J). $n = 3$, biological repeat, values are mean ± SEM, one-way ANOVA.
(L) Representative western blot images of voltage-dependent anion channel (VDAC), succinate dehydrogenase (SDHA), and prohibitins (PHBs) to analyze mitochondrial function in cells.
(M) Quantitative graph of VDAC, SDHA, and PHBs from (L). $n = 3$, biological repeat, values are mean ± SEM, one-way ANOVA.
(N) Representative Western blot images of HSP60, cytochrome *c* oxidase (COX) IV, and cytochrome *c* (Cyto C) to analyze mitochondrial function in human DA neurons.
(O) Quantitative graphs of HSP60, COX IV, and Cyto C from (N).
(P) Fluorescent microscopy images of the lysosomal intracellular activity assay.
(Q) Quantitative graph corresponding to the assay results from (P). $n = 9$, biological repeat, values are mean ± SEM, one-way ANOVA.
(R) Results data from the 20S proteasome assay. $n = 7$, biological repeat, values are mean ± SEM, one-way ANOVA.
n.s., non-significance.

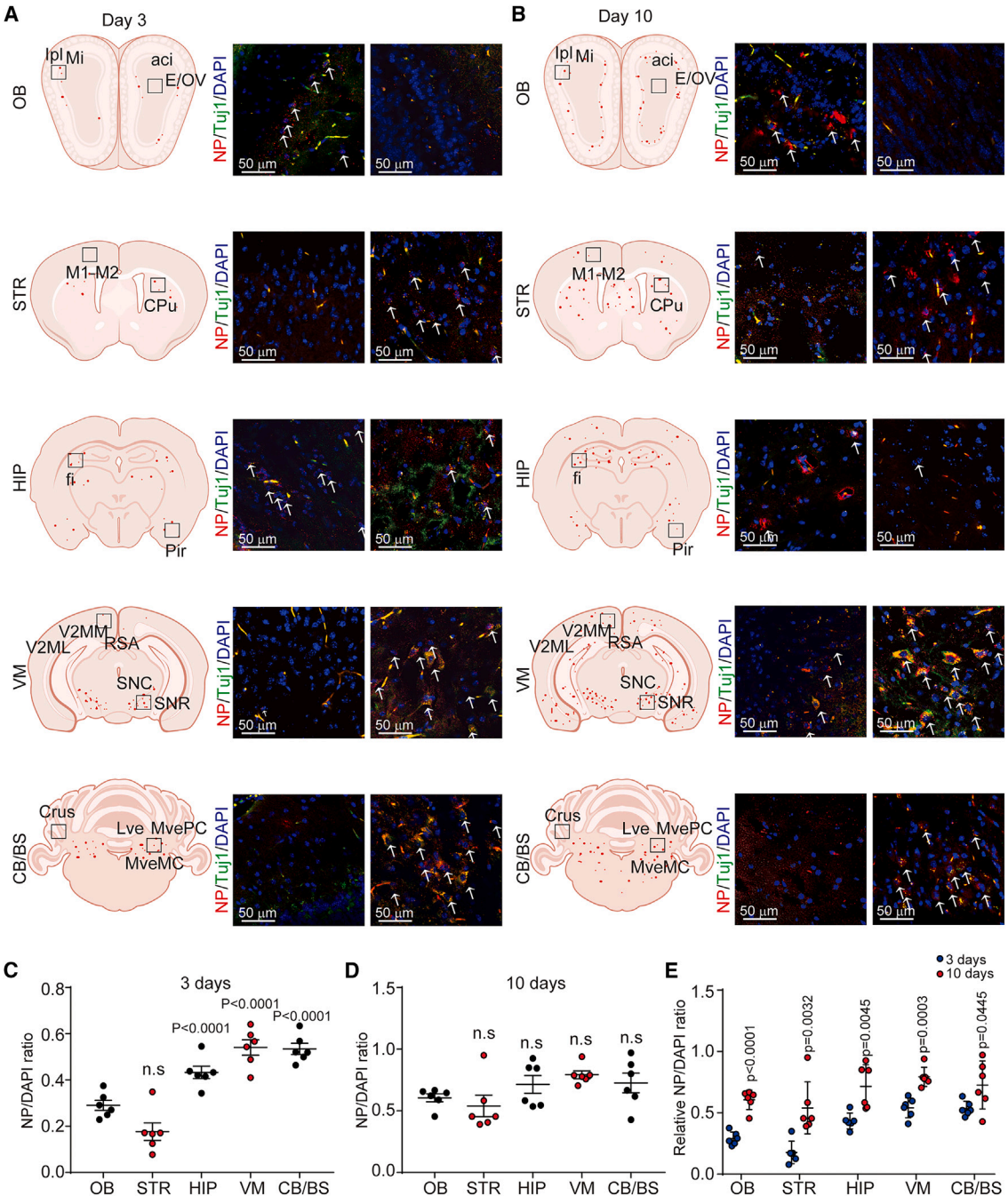

Figure 3. Brain mapping of mice infected with SARS-CoV-2

(A and B) Brain mapping of mice (A) 3 and (B) 10 days after 10^3 $TCID_{50}$ SARS-CoV-2 infection. Ipl, internal plexiform layer of the olfactory bulb (OB); Mi, mitral cell layer of the OB; eci, ependymal and subendymal layer/olfactory ventricle; E/OV, anterior commissure, intrabulbar part; M1, primary motor cortex; M2, secondary motor cortex; CPu, caudate putamen (STR); fi, fimbria of the hippocampus (HIP), Pri, piriform cortex; V2ML, secondary visual cortex, mediolateral area; V2MM, secondary visual cortex, mediomedial area; RSA, retrosplenial agranular cortex; SNC, substantia nigra, compact part; SNR, substantia nigra, reticular part; Crus, crus of the ansiform lobule; Lve, lateral vestibular nucleus; MvePC, medial vestibular nucleus, parvicellular; MveMC, medial vestibular nucleus, magnocellular.

(C) NP infection/DAPI ratio cell count graph in OB, STR, HIP, VM, and cerebrum (CB)/brain stem (BS) regions on day 3.

(D) NP infection/DAPI cell count ratio graph in the OB, STR, HIP, VM, and CB/BS regions on day 10.

(E) Comparison graph between day 3/10 NP infection/DAPI cell count ratio graphs in the OB, STR, HIP, VM, and CB/BS regions. $n = 3$, biological repeat, values are mean ± SEM, one-way ANOVA.

n.s., non-significance.

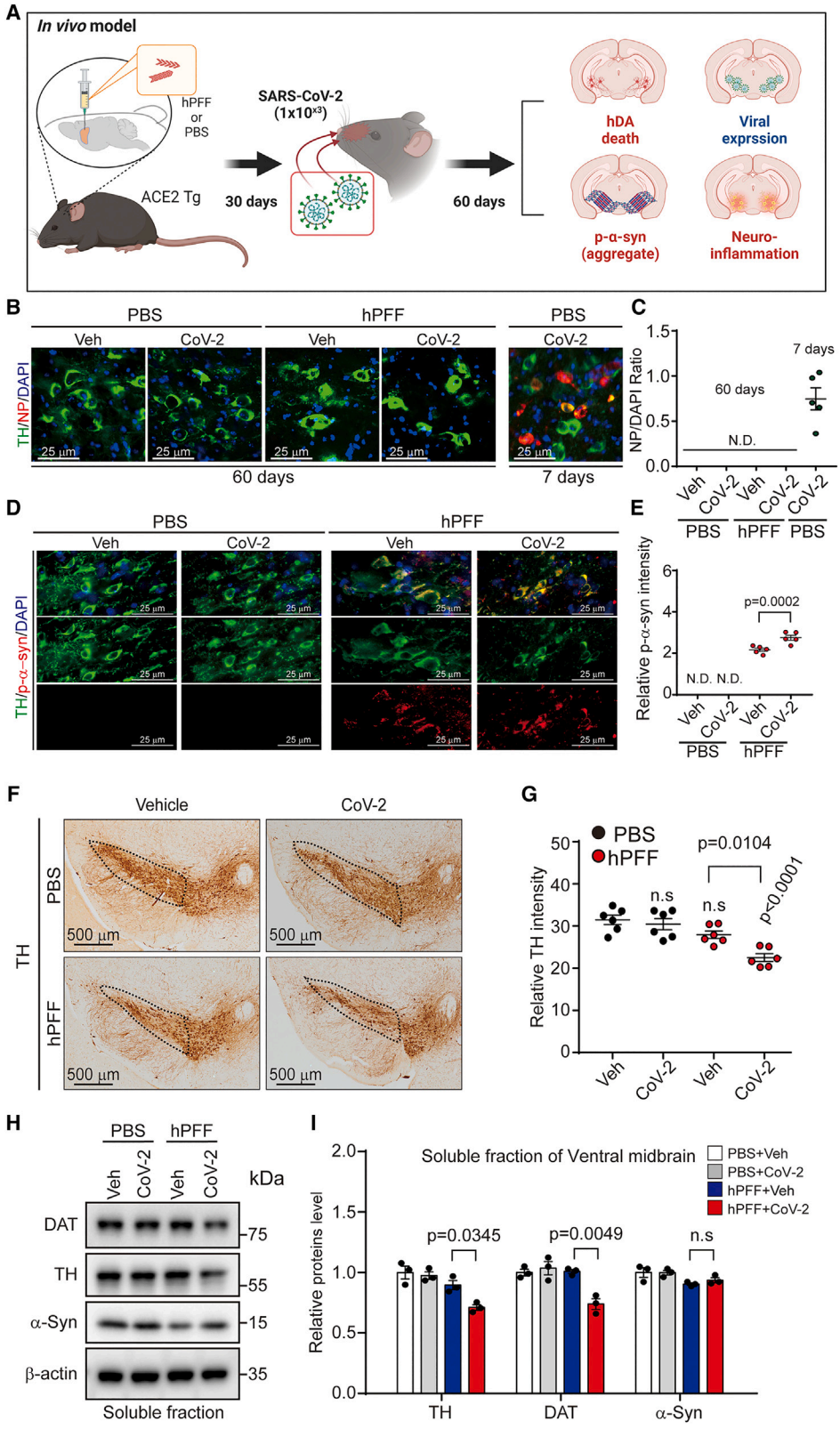

(legend on next page)

Amplification of hPFF-mediated neuroinflammation by SARS-CoV-2

We aimed to investigate the potential contribution of the inflammatory response within the neurological system to the heightened PD-like pathology induced by hPFFs in mice infected with SARS-CoV-2. In the SNpc and substantia nigra pars reticulata (SNr) brain regions, the expression of Iba-1 was upregulated in mice treated with both hPFFs and SARS-CoV-2 compared to those treated with hPFFs alone, as confirmed by IHC and western blotting (Figures 6A–6D). IHC analysis on the brains of mice treated with hPFFs followed by SARS-CoV-2 infection revealed significantly higher Iba-1 intensity values compared to mice treated with hPFFs alone. Both the hPFF-only treatment group and the SARS-CoV-2-infection-only group exhibited a substantial increase in Iba-1 compared to the vehicle control group. Notably, the group subjected to hPFF treatment followed by SARS-CoV-2 infection displayed a more pronounced increase in the level of Iba-1 compared to the hPFF-only group (Figures 6A and 6B). Furthermore, western blot analysis confirmed that the Iba-1 protein level was higher in mice infected with SARS-CoV-2 in addition to hPFF injection than in mice injected with hPFFs only. Both groups showed significant increases compared to the vehicle control, and the level of Iba-1 in the hPFF-with-SARS-CoV-2 group was significantly elevated compared to the hPFF-only group (Figures 6C and 6D). In qPCR analysis of VM, groups with hPFFs and SARS-CoV-2 showed a significant upregulation in the expression of cytokine genes (*Il1a*, *Tnf*, *C1qa*, *Il1b*, and *Il6*) associated with neuroinflammation (Figures 6E–6G, S7A, and S7B) compared to other groups. Similarly, in the STR, cytokine genes (*Il1a*, *Tnf*, *C1qa*, *Il1b*, and *Il6*) implicated in neuroinflammation were upregulated in the hPFF-with-SARS-CoV-2 group, with a trend similar to that in the VM (Figures S7C–S7G).

Moreover, GFAP expression was upregulated in the SNpc and SNr regions of mice treated with both hPFFs and SARS-CoV-2 compared to those treated with hPFFs alone (Figures 6H–6K). IHC and western blot analyses performed in the VM of the mouse brain demonstrated a substantial increase in GFAP intensity when hPFF-injected mice were infected with SARS-CoV-2 compared to mice injected with hPFFs alone (Figures 6H and 6I). The hPFF-with-SARS-CoV-2 group exhibited a significant increase in GFAP levels in contrast to the hPFF-only group (Figures 6J and 6K). The western blot results indicated that the increase in GFAP levels in the hPFF-with-SARS-CoV-2 group was approximately twice that in the hPFF-alone treatment group. Additionally, hPFF-induced toxic A1-specific transcripts and PAN-reactive transcripts were further enhanced with SARS-CoV-2 infection (Figures 6L and S8A; Tables S3 and S4). However, only *S100a10* and *ptgs2* A2-specific transcripts showed significant changes compared to hPFF treatment alone (Figure S8B; Table S4). These findings suggest that SARS-CoV-2 infection amplifies hPFF-induced PD pathological features.

SARS-CoV-2 infection regulates *in vivo* molecular features of PD progression induced by hPFFs

Importantly, the genetic pathological characteristics contributing to the progression of PD, observed in *in vitro* experiments using hDA neurons, were also detected in the brain of mice *in vivo*. Apoptosis-related genes (*FADD*, *BAX*, *BID*, and *CASP9*) and autophagy-related genes (*WDR45*, *TECPR2*, and *SQSTM1*) exhibited upregulation in both the VM (Figure S9) and STR (Figure S10) with hPFF treatment alone, with further amplification of these elevated levels observed upon additional SARS-CoV-2 infection. Upregulation of genes implicated in the onset of PD (*CYC1*, *COX7b*, *PRKACA*, *HAP1*, *WDR24*, *PIN1*, *PPP2CA*) induced by hPFFs were validated in the VM and STR, along with decreased level of genes for normal DA neuronal function (*TH* and *KIF5C*). These findings suggest that SARS-CoV-2 infection intensifies PD-like pathology mediated by hPFF deposition by exacerbating the alterations in genes associated with PD-like pathology. Given the similar results observed in brain regions relevant to PD (VM and STR) and in DA neurons, it is conceivable that SARS-CoV-2 could worsen molecular changes linked to PD progression across DA neuronal areas, especially under the influence of pathological factors such as hPFFs. This implies that, in the presence of PD pathological factors, SARS-CoV-2 may influence the molecular mechanisms of PD, potentially hastening the progression of the disease.

DISCUSSION

Our study aimed to unravel the complex interplay between SARS-CoV-2 infection and the pathology of PD. To contextualize our findings, it is essential to consider previous research associating various viruses, such as influenza virus H1N1 and HIV-1, with neurodegenerative diseases like PD.[35–37] The reported neuroinvasive potential of SARS-CoV-2 in peripheral nervous system infection aligns with these precedents,[38,39] prompting our investigation into the specific mechanisms linking SARS-CoV-2 and PD.

Figure 4. SARS-CoV-2 increased hPFF-induced PD-like pathology

(A) Schematic diagram of the SARS-CoV-2 (10^3 $TCID_{50}$) infection schedule in ACE2 Tg mice treated with hPFF.
(B) Representative immunofluorescence image of TH (green) and NP (red).
(C) NP/DAPI ratio of (B).
(D) Representative immunofluorescence image of TH (green) and p-α-Syn (red).
(E) Quantification of (D) p-α-Syn intensity in VM at 60 days. $n = 5$, biological repeat, values are mean ± SEM, one-way ANOVA.
(F) Representative TH immunohistochemistry images of the VM region of ACE2 Tg mice.
(G) Quantification of (F) TH intensity. $n = 6$, biological repeat, values are mean ± SEM, one-way ANOVA.
(H) Representative western blot bands of DAT, TH, α-Syn, and β-actin in VM tissue.
(I) Quantification of DAT, TH, and α-Syn levels from (H). $n = 3$, biological repeat, values are mean ± SEM, one-way ANOVA.
n.s., non-significance; N.D., non-detection.
See also Figure S4.

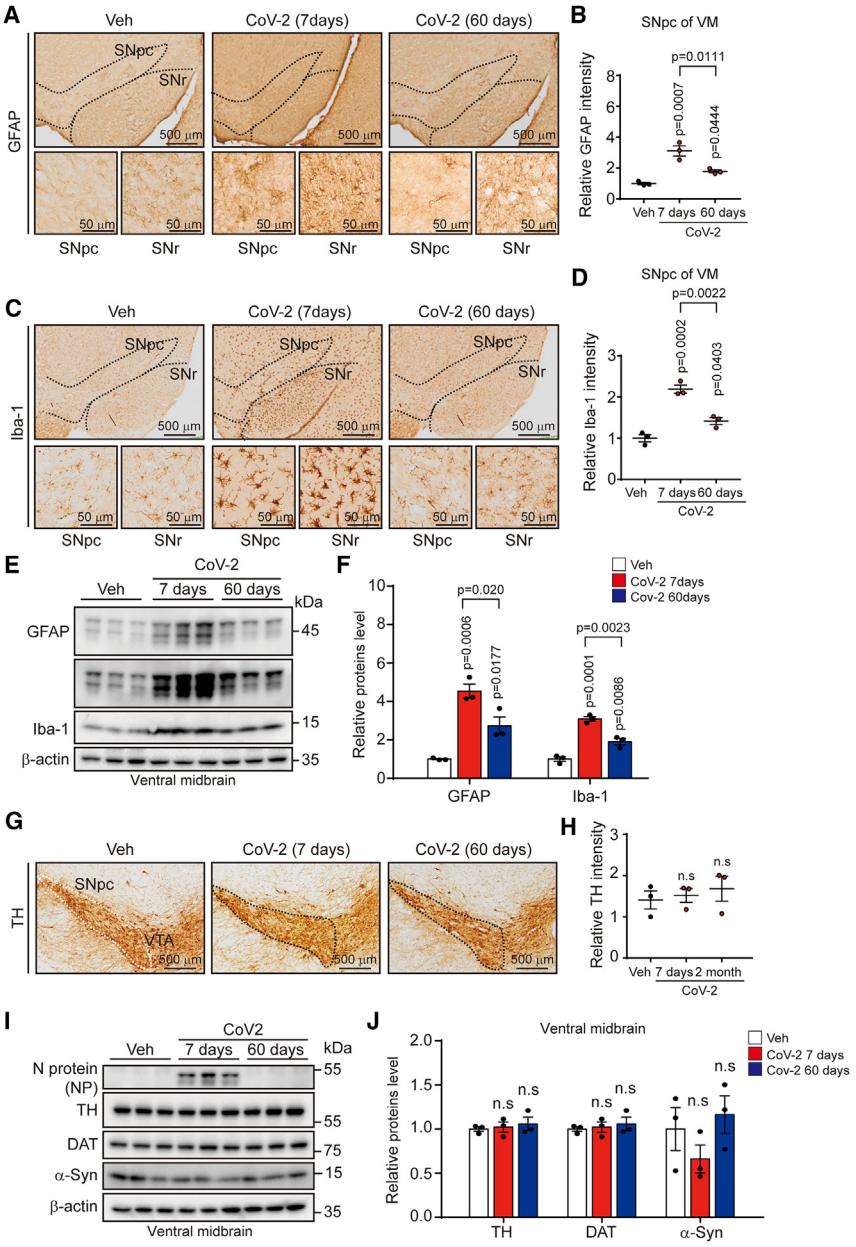

Figure 5. Infection with SARS-CoV-2 sustained the expression of GFAP and Iba-1 for 60 days

(A) Representative GFAP immunochemistry images of the VM region of ACE2 Tg mice infected with SARS-CoV-2 (10^3 $TCID_{50}$).

(B) Quantification of GFAP in the SNpc region. $n = 3$, biological repeat, values are mean ± SEM, one-way ANOVA.

(C) Representative Iba-1 immunochemistry images of the VM region of ACE2 Tg mice infected with SARS-CoV-2.

(D) Quantification of Iba-1 in the SNpc region. $n = 3$, biological repeat, values are mean ± SEM, one-way ANOVA.

(E) Representative western blot bands of GFAP and Iba-1 in the VM.

(F) Quantification of GFAP and Iba-1 western blot bands in the VM. $n = 3$, biological repeat, values are mean ± SEM, one-way ANOVA.

(G) Representative TH immunochemistry images of the VM region of ACE2 Tg mice infected with SARS-CoV-2.

(H) Quantification of GFAP in the SNpc region. $n = 3$, biological repeat, values are mean ± SEM, one-way ANOVA.

(I) Representative western blot bands of NP, TH, DAT, and α-Syn in VM after infection with SARS-CoV-2 for 7 and 60 days.

(J) Quantification of (I). $n = 3$, biological repeat, values are mean ± SEM, one-way ANOVA.

n.s., non-significance.

See also Figures S5 and S6.

In our *in vitro* experiments, we exposed hDA neurons to α-Syn aggregates (hPFFs) and subsequently infected them with SARS-CoV-2. The results unveiled a synergistic relationship, with SARS-CoV-2 exacerbating α-Syn pathology, marked by increased phosphorylation and heightened apoptotic cell death in hDA neurons (Figure 1). Transcriptome profiling further illustrated alterations in gene expression associated with neurodegenerative diseases, particularly PD (Figure 2). The *in vivo* experiments, utilizing hACE2 Tg mice, demonstrated the ability of SARS-CoV-2 to reach the brain, specifically affecting regions relevant to PD progression (Figure 3). Mice injected with hPFFs followed by SARS-CoV-2 infection exhibited exacerbated PD-like pathology, including increased phosphorylation of α-Syn, reduced expression of DA neuronal markers, and heightened neuroinflammation (Figure 4). Importantly, our study explored the persistence of SARS-CoV-2-induced neuroinflammation beyond the clearance of the virus. Prolonged activation of glial cells and increased expression of proinflammatory cytokines were observed up to 60 days post-infection, providing insight into a potential mechanism for persistent neurological symptoms in some COVID-19 patients (Figure 5). Comparative analysis of different SARS-CoV-2 variants emphasized the neuroinvasive potential of the virus, irrespective of specific viral variations (Figure 6). This comprehensive approach strengthens our understanding of the intricate relationship between SARS-CoV-2 and PD progression.

Recent cohort analyses support our experimental findings, indicating a statistically significant increase in PD incidence among individuals infected with SARS-CoV-2 within 1–2 years, though the magnitude of the increase is minimal.[40–42] Considering the long and gradual onset of PD, it is anticipated that these trends will become more apparent over time. While clinical observational studies have explored the associations between SARS-CoV-2 infection and neurological

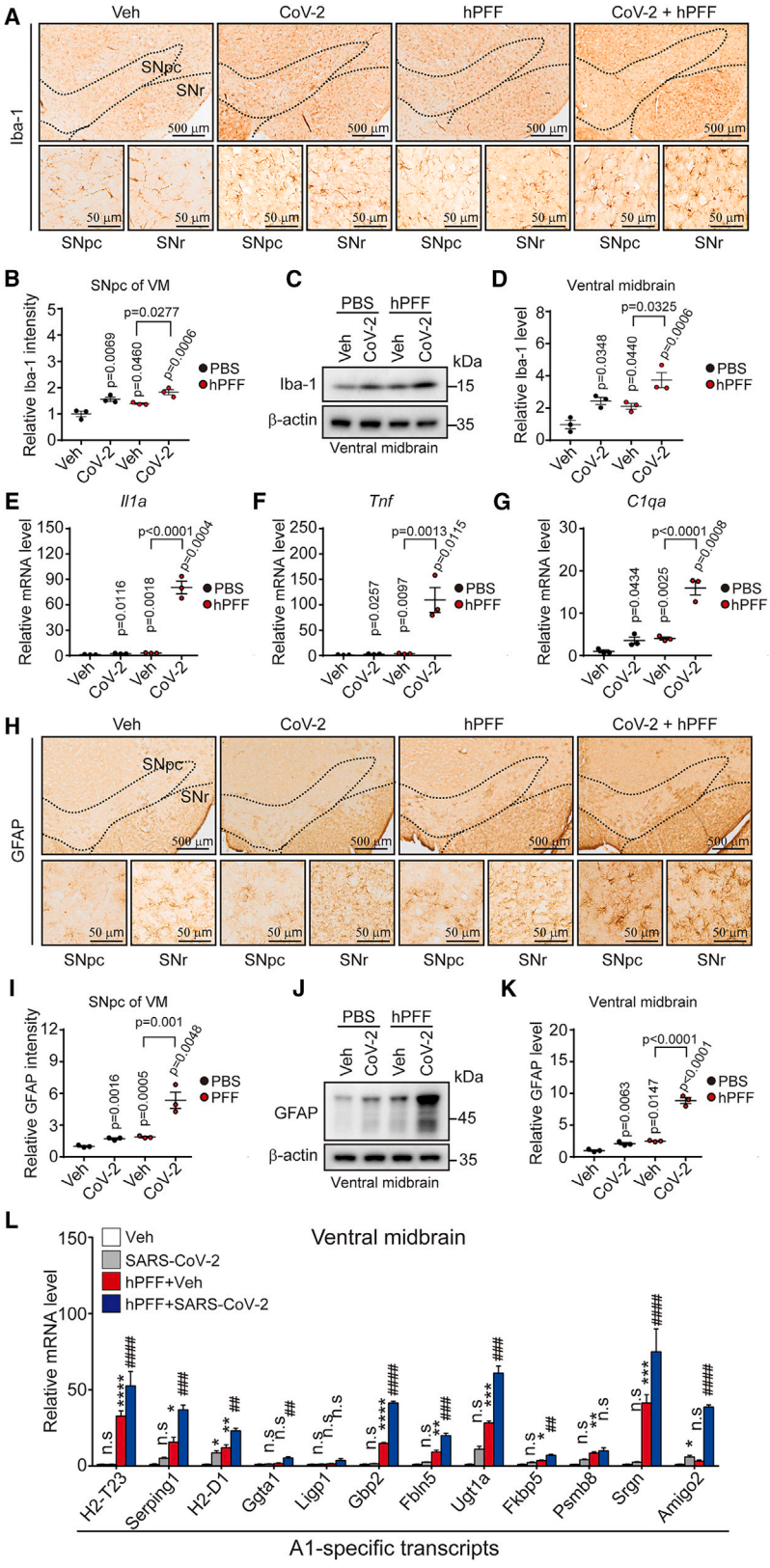

Figure 6. SARS-CoV-2 infection upregulates hPFF-induced Iba-1 and GFAP expression in the VM, and this effect persists even after 60 days

(A) Representative Iba-1 IHC images of the VM SNpc and SNr regions.

(B) Quantification of Iba-1 levels. $n = 3$, biological repeat, values are mean ± SEM, one-way ANOVA.

(C) Representative western blot band of Iba-1 in the VM.

(D) Quantification of Iba-1 expression levels from (C). $n = 3$, biological repeat, values are mean ± SEM, one-way ANOVA.

(E–G) qPCR analysis of the VM in hPFF-injected mice treated with vehicle or SARS-CoV-2 for *Il1a*, *Tnf*, and *C1qa*. $n = 3$, biological repeat, values are mean ± SEM, one-way ANOVA.

(H) Representative GFAP immunochemistry images of the SNpc and SNr regions.

(I) Quantification of GFAP levels. $n = 3$, biological repeat, values are mean ± SEM, one-way ANOVA.

(J) Representative western blot band of GFAP in the VM.

(K) Quantification of GFAP expression levels from (J). $n = 3$, biological repeat, values are mean ± SEM, one-way ANOVA.

(L) qPCR analysis of the VM in hPFF-injected mice treated with vehicle or SARS-CoV-2 for A1-specific transcripts. $n = 3$, biological repeat, values are mean ± SEM, one-way ANOVA.

n.s., non-significance.

See also Figures S7–S10.

diseases,[43–45] there remains an unmet need for mechanistic studies elucidating how SARS-CoV-2 facilitates the onset of PD. Postmortem studies have revealed elevated levels of proinflammatory cytokines such as tumor necrosis factor, interleukin (IL)-1, and IL-6, suggesting a potential acute onset of PD mediated by neuroinflammation in individuals with preexisting risk factors.[45,46] Additionally, SARS-CoV-2 could invade the brain directly or indirectly through immune cell infiltration, bloodstream routes, or neural pathways, potentially connecting to brain neuroinflammation.[47,48] Indeed, approximately 18% of SARS-CoV-2-infected individuals exhibit neurological symptoms such as encephalopathy, encephalitis, cerebrovascular pathology, and acute myelitis, among others.[49,50]

Our research underscores the imperative to focus on patients with neurodegenerative disorders post-resolution of COVID-19 and develop effective management strategies. The findings suggest that SARS-CoV-2 may exacerbate or accelerate the manifestation of symptoms in patients with preexisting PD progression risk factors by inducing short-term DA neuronal injury and prolonged activation of glial cells. Based on experimental evidence from our results, revealing sustained glial cell-induced inflammation in the brain even 60 days after undetectable SARS-CoV-2 infection, we propose the necessity of longitudinally tracking neuroinflammation in the brain for individuals who have experienced SARS-CoV-2 infection and belong to potential PD risk groups. This suggestion aligns with a recent study using a 1-methyl-4-phenyl-1,2,3,6-tetrahydropyridine (MPTP)-induced PD mouse model, which found an aggravation of neuronal loss and microgliosis with dual treatment following SARS-CoV-2 infection.[51] This observation, unique to SARS-CoV-2 and not occurring in the case of other neurotropic viruses (Figure S11), underscores the importance of directing attention to the aftermath of the COVID-19 pandemic, particularly in terms of lingering effects, unlike other viral infections. Specifically, our transcriptome analysis suggests that when hDA neurons with a risk of PD are exposed to additional stimuli from SARS-CoV-2 infection, signaling pathways contributing to PD onset,[52–55] such as fibroblast growth factor, wingless/int1 (WNT), bone morphogenetic protein (BMP), and insulin pathways, become activated (Tables S1 and S2). This implies an opportunity to target these pathways, potentially interrupting the link between COVID-19 and the acceleration of PD progression, as indicated by our findings. In our study, we demonstrated that SARS-CoV-2 infection exacerbated PD progression induced by hPFF treatment and promoted decreased expressions of DA neuronal markers in an ACE2 Tg mouse model. Surprisingly, even after 60 days post-infection, when SARS-CoV-2 had cleared with no detectable virus remaining, persistent activation of GFAP and IBA-1 was observed within the brain. Furthermore, through additional experiments, it has been confirmed that the features of long-term neuroinflammation are associated with SARS-CoV-2 infection and are not present in other neuroactive viruses (Figure S11). This suggests that the SARS-CoV-2 virus-induced neuroinflammation response continued to affect the brain over an extended period. A recent study using another model of PD (MPTP treatment) of mice following SARS-CoV-2 infection found an aggravation of neuronal loss and microgliosis with dual treatment[51] comparable to our findings.

Limitations of the study

Our study encounters limitations that necessitate identifying specific molecular mechanisms through which SARS-CoV-2 infection triggers prolonged maintenance of glial cell activity. The critical task at hand is determining whether this activation ultimately correlates with behavioral changes, such as motor function decline in PD models, especially during periods relevant to human aging. We expect that advancements in technology, including the utilization of recent stem cell or organoid models to simulate the onset and progression of PD,[56–58] along with the incorporation of human glial cells,[59] will facilitate studies in uncovering more precise mechanisms in the future. Our study established α-Syn as a preexisting risk factor for the exacerbation of PD progression induced by SARS-CoV-2 infection. However, considering recent studies indicating the contribution of leucine-rich repeat kinase (LRRK) mutations to tauopathy and its role in PD onset,[60,61] a limitation arises from the exclusion of other aggregates, such as tau, as additional risk factors. This limitation impedes the assessment of the overall contribution of protein aggregation phenomena in the correlation between SARS-CoV-2 and PD progression. Another limitation of our study is the lack of validation through clinical epidemiological data from patients, given that PD progresses over a relatively long period. This requires more robust validation in numerous individuals across animal models, as our research utilized a manageable number of individuals under limited conditions. We expect the significance of our findings to be enhanced through future extensive patient cohort collection and analysis, along with large-scale animal studies conducted over extended periods.

Conclusion

We investigated the potential for an accelerated onset and progression of PD following recovery from short-term SARS-CoV-2 infection, considering extensive literature that links viral infections to the exacerbation of PD.[43–45] In this context, we observed that the neuroinflammatory response remains sustained even when SARS-CoV-2 is no longer detectable in the brain. This suggests that the impact of SARS-CoV-2 infection may extend beyond acute COVID-19-associated parkinsonism, as reported in recent case studies,[43–45] potentially affecting those with existing PD diagnoses or those exposed to PD risk factors. Moreover, such infections could conceivably contribute to a higher incidence of PD in future years. This is of concern as a potential public health issue given the widespread prevalence of SARS-CoV-2 infections globally.

STAR★METHODS

Detailed methods are provided in the online version of this paper and include the following:

- KEY RESOURCES TABLE
- RESOURCE AVAILABILITY
  - Lead contact
  - Materials availability

SUPPLEMENTAL INFORMATION

Supplemental information can be found online at https://doi.org/10.1016/j.xcrm.2024.101570.

ACKNOWLEDGMENTS

Work in the Yun lab was supported by the National Research Foundation of Korea (NRF-2021R1A4A3027122, 2023R1A2C2004516, and RS-2023-00219399). Work in the Kim lab was supported by the Korean Fund for Regenerative Medicine (KFRM) grant funded by the Korean government (the Ministry of Science and ICT, the Ministry of Health & Welfare) (2021M3E5E5096744); the National Research Foundation of Korea (NRF-2022R1A2C1091779, NRF-2022R1A2C109177, NRF-2023R1A2C007120, and RS-2023-00266171); the Korea Health Technology R&D Project through the Korea Health Industry Development Institute (KHIDI) funded by the Korean Ministry of Health & Welfare (HI23C126300); and the KIST Institutional Program (project no. 2Z05790-19-037). Work in the Lee lab was supported by the National Research Foundation of Korea (2022R1I1A1A01063511). Work in the Roh lab was supported by a grant from the Animal and Plant Quarantine Agency of the Republic of Korea (grant no. B-1543085-2022-23-01).

AUTHOR CONTRIBUTIONS

Study design and data analysis, B.L., H.N.C., Y.H.C., K.-S.L., Yong Jun Kim, and S.P.Y.; performed experiments, B.L., H.N.C., Y.H.C., S.Y., J.H.K., Young Jin Kim, and Yong Jun Kim; interpretation, M.K. and S.P.Y.; conception, study design, and data analysis, H.M.S., M.G.J., S.-H.K., C.S., S.-G.Y., K.-W.H., and I.-S.R.; conception, data analysis, and assembly, M.K., M.Y.L., S.W.P., and H.J.K.; assembly, interpretation, and manuscript writing, M.K., D.S.M., R.G.E., S.J.K., S.L., J.-H.P., and Yong Jun Kim.

DECLARATION OF INTERESTS

The authors declare no competing interests.

Received: June 20, 2023
Revised: January 23, 2024
Accepted: April 22, 2024
Published: May 14, 2024

REFERENCES

1. Krammer, F. (2020). SARS-CoV-2 vaccines in development. Nature *586*, 516–527. https://doi.org/10.1038/s41586-020-2798-3.
2. Benameur, K., Agarwal, A., Auld, S.C., Butters, M.P., Webster, A.S., Ozturk, T., Howell, J.C., Bassit, L.C., Velasquez, A., Schinazi, R.F., et al. (2020). Encephalopathy and Encephalitis Associated with Cerebrospinal Fluid Cytokine Alterations and Coronavirus Disease, Atlanta, Georgia, USA, 2020. Emerg. Infect. Dis. *26*, 2016–2021. https://doi.org/10.3201/eid2609.202122.
3. Zhang, P.P., He, Z.C., Yao, X.H., Tang, R., Ma, J., Luo, T., Zhu, C., Li, T.R., Liu, X., Zhang, D., et al. (2023). COVID-19-associated monocytic encephalitis (CAME): histological and proteomic evidence from autopsy. Signal Transduct. Target. Ther. *8*, 24. https://doi.org/10.1038/s41392-022-01291-6.
4. Sonneville, R., Dangayach, N.S., and Newcombe, V. (2023). Neurological complications of critically ill COVID-19 patients. Curr. Opin. Crit. Care *29*, 61–67. https://doi.org/10.1097/MCC.0000000000001029.
5. Guilmot, A., Maldonado Slootjes, S., Sellimi, A., Bronchain, M., Hanseeuw, B., Belkhir, L., Yombi, J.C., De Greef, J., Pothen, L., Yildiz, H., et al. (2021). Immune-mediated neurological syndromes in SARS-CoV-2-infected patients. J. Neurol. *268*, 751–757. https://doi.org/10.1007/s00415-020-10108-x.
6. Ahmed, M., Roy, S., Iktidar, M.A., Chowdhury, S., Akhter, S., Khairul Islam, A.M., and Hawlader, M.D.H. (2022). Post-COVID-19 Memory Complaints: Prevalence and Associated Factors. Neurologia *1234*. https://doi.org/10.1016/j.nrl.2022.03.007.
7. Tana, C., Bentivegna, E., Cho, S.J., Harriott, A.M., García-Azorín, D., Labastida-Ramirez, A., Ornello, R., Raffaelli, B., Beltrán, E.R., Ruscheweyh, R., and Martelletti, P. (2022). Long COVID headache. J. Headache Pain *23*, 93. https://doi.org/10.1186/s10194-022-01450-8.
8. Tanasa, I.A., Manciuc, C., Carauleanu, A., Navolan, D.B., Bohiltea, R.E., and Nemescu, D. (2020). Anosmia and ageusia associated with coronavirus infection (COVID-19) - what is known? Exp. Ther. Med. *20*, 2344–2347. https://doi.org/10.3892/etm.2020.8808.
9. Douaud, G., Lee, S., Alfaro-Almagro, F., Arthofer, C., Wang, C., McCarthy, P., Lange, F., Andersson, J.L.R., Griffanti, L., Duff, E., et al. (2022). SARS-CoV-2 is associated with changes in brain structure in UK Biobank. Preprint at medRxiv *1234*. https://doi.org/10.1101/2021.06.11.21258690.
10. Cavallieri, F., Fioravanti, V., Bove, F., Del Prete, E., Meoni, S., Grisanti, S., Zedde, M., Pascarella, R., Moro, E., and Valzania, F. (2022). COVID-19 and Parkinsonism: A Critical Appraisal. Biomolecules *12*, 970. https://doi.org/10.3390/biom12070970.
11. Meinhardt, J., Radke, J., Dittmayer, C., Franz, J., Thomas, C., Mothes, R., Laue, M., Schneider, J., Brünink, S., Greuel, S., et al. (2021). Olfactory transmucosal SARS-CoV-2 invasion as a port of central nervous system entry in individuals with COVID-19. Nat. Neurosci. *24*, 168–175. https://doi.org/10.1038/s41593-020-00758-5.
12. Sulzer, D., Antonini, A., Leta, V., Nordvig, A., Smeyne, R.J., Goldman, J.E., Al-Dalahmah, O., Zecca, L., Sette, A., Bubacco, L., et al. (2020). COVID-19 and possible links with Parkinson's disease and parkinsonism: from bench to bedside. NPJ Parkinsons Dis. *6*, 18. https://doi.org/10.1038/s41531-020-00123-0.
13. Pilotto, A., Masciocchi, S., Volonghi, I., De Giuli, V., Caprioli, F., Mariotto, S., Ferrari, S., Bozzetti, S., Imarisio, A., Risi, B., et al. (2021). Severe Acute Respiratory Syndrome Coronavirus 2 (SARS-CoV-2) Encephalitis Is a Cytokine Release Syndrome: Evidences From Cerebrospinal Fluid Analyses. Clin. Infect. Dis. *73*, e3019–e3026. https://doi.org/10.1093/cid/ciaa1933.
14. Kanberg, N., Simrén, J., Edén, A., Andersson, L.M., Nilsson, S., Ashton, N.J., Sundvall, P.D., Nellgård, B., Blennow, K., Zetterberg, H., and Gisslén, M. (2021). Neurochemical signs of astrocytic and neuronal injury in acute

COVID-19 normalizes during long-term follow-up. EBioMedicine *70*, 103512. https://doi.org/10.1016/j.ebiom.2021.103512.

15. Calculli, A., Bocci, T., Porcino, M., Avenali, M., Casellato, C., Arceri, S., Regalbuto, S., Priori, A., and Pisani, A. (2023). Parkinson disease following COVID-19: Report of six cases. Eur. J. Neurol. *30*, 1272–1280. https://doi.org/10.1111/ene.15732.
16. Rao, A.R., Hidayathullah, S.M., Hegde, K., and Adhikari, P. (2022). Parkinsonism: An emerging post COVID sequelae. IDCases *27*, e01388. https://doi.org/10.1016/j.idcr.2022.e01388.
17. Wang, H., Liu, X., Tan, C., Zhou, W., Jiang, J., Peng, W., Zhou, X., Mo, L., and Chen, L. (2020). Bacterial, viral, and fungal infection-related risk of Parkinson's disease: Meta-analysis of cohort and case-control studies. Brain Behav. *10*, e01549. https://doi.org/10.1002/brb3.1549.
18. Garg, R.K., Mahadevan, A., Malhotra, H.S., Rizvi, I., Kumar, N., and Uniyal, R. (2019). Subacute sclerosing panencephalitis. Rev. Med. Virol. *29*, e2058. https://doi.org/10.1002/rmv.2058.
19. Jafri, S.K., Kumar, R., and Ibrahim, S.H. (2018). Subacute sclerosing panencephalitis - current perspectives. Pediatric Health Med. Ther. *9*, 67–71. https://doi.org/10.2147/PHMT.S126293.
20. Lopez, G., Tonello, C., Osipova, G., Carsana, L., Biasin, M., Cappelletti, G., Pellegrinelli, A., Lauri, E., Zerbi, P., Rossi, R.S., and Nebuloni, M. (2022). Olfactory bulb SARS-CoV-2 infection is not paralleled by the presence of virus in other central nervous system areas. Neuropathol. Appl. Neurobiol. *48*, e12752. https://doi.org/10.1111/nan.12752.
21. Jarazo, J., da Silva, E.S., Glaab, E., Perez-Bercoff, D., and Schwamborn, J.C. (2023). SARS-CoV-2 infection induces dopaminergic neuronal loss in midbrain organoids during short and prolonged cultures. Preprint at bioRxiv. https://doi.org/10.1101/2023.03.20.533485.
22. Han, Y., Yang, L., Kim, T.W., Nair, M.S., Harschnitz, O., Wang, P., Zhu, J., Koo, S.Y., Tang, X., Lacko, L.A., et al. (2021). SARS-CoV-2 Infection Causes Dopaminergic Neuron Senescence. Preprint at Res. Sq. *1234*. https://doi.org/10.21203/rs.3.rs-513461/v1.
23. Abdelmotilib, H., Maltbie, T., Delic, V., Liu, Z., Hu, X., Fraser, K.B., Moehle, M.S., Stoyka, L., Anabtawi, N., Krendelchtchikova, V., et al. (2017). alpha-Synuclein fibril-induced inclusion spread in rats and mice correlates with dopaminergic Neurodegeneration. Neurobiol. Dis. *105*, 84–98. https://doi.org/10.1016/j.nbd.2017.05.014.
24. Tarutani, A., Suzuki, G., Shimozawa, A., Nonaka, T., Akiyama, H., Hisanaga, S.I., and Hasegawa, M. (2016). The Effect of Fragmented Pathogenic alpha-Synuclein Seeds on Prion-like Propagation. J. Biol. Chem. *291*, 18675–18688. https://doi.org/10.1074/jbc.M116.734707.
25. Tatton, W.G., Chalmers-Redman, R., Brown, D., and Tatton, N. (2003). Apoptosis in Parkinson's disease: signals for neuronal degradation. Ann. Neurol. *53*, S61–S72, discussion S70-62. https://doi.org/10.1002/ana.10489.
26. Xiong, Q., Li, X., Li, W., Chen, G., Xiao, H., Li, P., and Wu, C. (2021). WDR45 Mutation Impairs the Autophagic Degradation of Transferrin Receptor and Promotes Ferroptosis. Front. Mol. Biosci. *8*, 645831. https://doi.org/10.3389/fmolb.2021.645831.
27. Oz-Levi, D., Gelman, A., Elazar, Z., and Lancet, D. (2013). TECPR2: a new autophagy link for neurodegeneration. Autophagy *9*, 801–802. https://doi.org/10.4161/auto.23961.
28. Uddin, M.S., Stachowiak, A., Mamun, A.A., Tzvetkov, N.T., Takeda, S., Atanasov, A.G., Bergantin, L.B., Abdel-Daim, M.M., and Stankiewicz, A.M. (2018). Autophagy and Alzheimer's Disease: From Molecular Mechanisms to Therapeutic Implications. Front. Aging Neurosci. *10*, 4. https://doi.org/10.3389/fnagi.2018.00004.
29. Liu, Y., Huang, Q., Wei, Z., Ma, S., Woodgett, J.R., Li, M., and Li, J. (2021). GSK-3 mediates nuclear translocation of p62/SQSTM1 in MPTP-induced mouse model of Parkinson's disease. Neurosci. Lett. *763*, 136177. https://doi.org/10.1016/j.neulet.2021.136177.
30. Kwon, D.N., Park, W.J., Choi, Y.J., Gurunathan, S., and Kim, J.H. (2015). Oxidative stress and ROS metabolism via down-regulation of sirtuin 3 expression in Cmah-null mice affect hearing loss. Aging (Albany NY) *7*, 579–594. https://doi.org/10.18632/aging.100800.
31. Gupta, R.C. (2019). Biomarkers in Toxicology, 2nd Edition (Academic Press/Elsevier).
32. Gan, L., Seki, A., Shen, K., Iyer, H., Han, K., Hayer, A., Wollman, R., Ge, X., Lin, J.R., Dey, G., et al. (2019). The lysosomal GPCR-like protein GPR137B regulates Rag and mTORC1 localization and activity. Nat. Cell Biol. *21*, 614–626. https://doi.org/10.1038/s41556-019-0321-6.
33. Walkinshaw, E., Gai, Y., Farkas, C., Richter, D., Nicholas, E., Keleman, K., and Davis, R.L. (2015). Identification of genes that promote or inhibit olfactory memory formation in Drosophila. Genetics *199*, 1173–1182. https://doi.org/10.1534/genetics.114.173575.
34. Shefa, U., Jeong, N.Y., Song, I.O., Chung, H.J., Kim, D., Jung, J., and Huh, Y. (2019). Mitophagy links oxidative stress conditions and neurodegenerative diseases. Neural Regen. Res. *14*, 749–756. https://doi.org/10.4103/1673-5374.249218.
35. Jurgens, H.A., Amancherla, K., and Johnson, R.W. (2012). Influenza infection induces neuroinflammation, alters hippocampal neuron morphology, and impairs cognition in adult mice. J. Neurosci. *32*, 3958–3968. https://doi.org/10.1523/JNEUROSCI.6389-11.2012.
36. Brew, B.J., Crowe, S.M., Landay, A., Cysique, L.A., and Guillemin, G. (2009). Neurodegeneration and ageing in the HAART era. J. Neuroimmune Pharmacol. *4*, 163–174. https://doi.org/10.1007/s11481-008-9143-1.
37. Bu, X.L., Wang, X., Xiang, Y., Shen, L.L., Wang, Q.H., Liu, Y.H., Jiao, S.S., Wang, Y.R., Cao, H.Y., Yi, X., et al. (2015). The association between infectious burden and Parkinson's disease: A case-control study. Parkinsonism Relat. Disord. *21*, 877–881. https://doi.org/10.1016/j.parkreldis.2015.05.015.
38. Lyoo, K.S., Kim, H.M., Lee, B., Che, Y.H., Kim, S.J., Song, D., Hwang, W., Lee, S., Park, J.H., Na, W., et al. (2022). Direct neuronal infection of SARS-CoV-2 reveals cellular and molecular pathology of chemosensory impairment of COVID-19 patients. Emerg. Microbes Infect. *11*, 406–411. https://doi.org/10.1080/22221751.2021.2024095.
39. Kurapati, S., Sadaoka, T., Rajbhandari, L., Jagdish, B., Shukla, P., Ali, M.A., Kim, Y.J., Lee, G., Cohen, J.I., and Venkatesan, A. (2017). Role of the JNK Pathway in Varicella-Zoster Virus Lytic Infection and Reactivation. J. Virol. *91*, e00640-17. https://doi.org/10.1128/JVI.00640-17.
40. Hu, Y., Yang, H., Hou, C., Chen, W., Zhang, H., Ying, Z., Hu, Y., Sun, Y., Qu, Y., Feychting, M., et al. (2022). COVID-19 related outcomes among individuals with neurodegenerative diseases: a cohort analysis in the UK biobank. BMC Neurol. *22*, 15. https://doi.org/10.1186/s12883-021-02536-7.
41. Wang, A.S., Perez, J.A., and Gunzler, S.A. (2023). Frequency of Parkinson disease following COVID-19 infection: A two-year retrospective cohort study. Parkinsonism Relat. Disord. *111*, 105433. https://doi.org/10.1016/j.parkreldis.2023.105433.
42. Xu, E., Xie, Y., and Al-Aly, Z. (2022). Long-term neurologic outcomes of COVID-19. Nat. Med. *28*, 2406–2415. https://doi.org/10.1038/s41591-022-02001-z.
43. Ayele, B.A., Demissie, H., Awraris, M., Amogne, W., Shalash, A., Ali, K., Zenebe, Y., Tafesse, A., and Venkatasubba Rao, C.P. (2021). SARS-COV-2 induced Parkinsonism: The first case from the sub-Saharan Africa. Clin. Park. Relat. Disord. *5*, 100116. https://doi.org/10.1016/j.prdoa.2021.100116.
44. Cavallieri, F., Fioravanti, V., Toschi, G., Grisanti, S., Napoli, M., Moratti, C., Pascarella, R., Versari, A., Fraternali, A., Casali, M., et al. (2022). COVID-19 and Parkinson's disease: a casual association or a possible second hit in neurodegeneration? J. Neurol. *269*, 59–61. https://doi.org/10.1007/s00415-021-10694-4.
45. Cohen, M.E., Eichel, R., Steiner-Birmanns, B., Janah, A., Ioshpa, M., Bar-Shalom, R., Paul, J.J., Gaber, H., Skrahina, V., Bornstein, N.M., and

Yahalom, G. (2020). A case of probable Parkinson's disease after SARS-CoV-2 infection. Lancet Neurol. *19*, 804–805. https://doi.org/10.1016/S1474-4422(20)30305-7.

46. Ali, S.S., Mumtaz, A., Qamar, M.A., Tebha, S.S., Parhin, A., Butt, M., and Essar, M.Y. (2022). New-onset Parkinsonism as a Covid-19 infection sequela: A systematic review and meta-analysis. Ann. Med. Surg. *80*, 104281. https://doi.org/10.1016/j.amsu.2022.104281.

47. Song, E., Zhang, C., Israelow, B., Lu-Culligan, A., Prado, A.V., Skriabine, S., Lu, P., Weizman, O.E., Liu, F., Dai, Y., et al. (2021). Neuroinvasion of SARS-CoV-2 in human and mouse brain. J. Exp. Med. *218*, e20202135. https://doi.org/10.1084/jem.20202135.

48. Kim, J., Koo, B.K., and Clevers, H. (2022). Organoid Studies in COVID-19 Research. Int. J. Stem Cells *15*, 3–13. https://doi.org/10.15283/ijsc21251.

49. Yachou, Y., El Idrissi, A., Belapasov, V., and Ait Benali, S. (2020). Neuroinvasion, neurotropic, and neuroinflammatory events of SARS-CoV-2: understanding the neurological manifestations in COVID-19 patients. Neurol. Sci. *41*, 2657–2669. https://doi.org/10.1007/s10072-020-04575-3.

50. Krey, L., Huber, M.K., Höglinger, G.U., and Wegner, F. (2021). Can SARS-CoV-2 Infection Lead to Neurodegeneration and Parkinson's Disease? Brain Sci. *11*, 1654. https://doi.org/10.3390/brainsci11121654.

51. Smeyne, R.J., Eells, J.B., Chatterjee, D., Byrne, M., Akula, S.M., Sriramula, S., O'Rourke, D.P., and Schmidt, P. (2022). COVID-19 Infection Enhances Susceptibility to Oxidative Stress-Induced Parkinsonism. Mov. Disord. *37*, 1394–1404. https://doi.org/10.1002/mds.29116.

52. Shin, J., Toyoda, S., Nishitani, S., Onodera, T., Fukuda, S., Kita, S., Fukuhara, A., and Shimomura, I. (2022). SARS-CoV-2 infection impairs the insulin/IGF signaling pathway in the lung, liver, adipose tissue, and pancreatic cells via IRF1. Metabolism *133*, 155236. https://doi.org/10.1016/j.metabol.2022.155236.

53. Tang, X.Y., Wu, S., Wang, D., Chu, C., Hong, Y., Tao, M., Hu, H., Xu, M., Guo, X., and Liu, Y. (2022). Human organoids in basic research and clinical applications. Signal Transduct. Target. Ther. *7*, 168. https://doi.org/10.1038/s41392-022-01024-9.

54. Arenas, E. (2014). Wnt signaling in midbrain dopaminergic neuron development and regenerative medicine for Parkinson's disease. J. Mol. Cell Biol. *6*, 42–53. https://doi.org/10.1093/jmcb/mju001.

55. Meyers, E.A., and Kessler, J.A. (2017). TGF-beta Family Signaling in Neural and Neuronal Differentiation, Development, and Function. Cold Spring Harb. Perspect. Biol. *9*, a022244. https://doi.org/10.1101/cshperspect.a022244.

56. Kim, M.S., Yoon, S., Choi, J., Kim, Y.J., and Lee, G. (2024). Stem Cell-Based Approaches in Parkinson's Disease Research. Int. J. Stem Cells *1234*. https://doi.org/10.15283/ijsc23169.

57. Che, Y.H., Choi, I.Y., Song, C.E., Park, C., Lim, S.K., Kim, J.H., Sung, S.H., Park, J.H., Lee, S., and Kim, Y.J. (2023). Peripheral Neuron-Organoid Interaction Induces Colonic Epithelial Differentiation via Non-Synaptic Substance P Secretion. Int. J. Stem Cells *16*, 269–280. https://doi.org/10.15283/ijsc23026.

58. Mukherjee-Clavin, B., Mi, R., Kern, B., Choi, I.Y., Lim, H., Oh, Y., Lannon, B., Kim, K.J., Bell, S., Hur, J.K., et al. (2019). Comparison of three congruent patient-specific cell types for the modelling of a human genetic Schwann-cell disorder. Nat. Biomed. Eng. *3*, 571–582. https://doi.org/10.1038/s41551-019-0381-8.

59. Yun, W., Kim, Y.J., and Lee, G. (2022). Direct Conversion to Achieve Glial Cell Fates: Oligodendrocytes and Schwann Cells. Int. J. Stem Cells *15*, 14–25. https://doi.org/10.15283/ijsc22008.

60. Herbst, S., Lewis, P.A., and Morris, H.R. (2022). The emerging role of LRRK2 in tauopathies. Clin. Sci. *136*, 1071–1079. https://doi.org/10.1042/CS20220067.

61. Zhang, X., Gao, F., Wang, D., Li, C., Fu, Y., He, W., and Zhang, J. (2018). Tau Pathology in Parkinson's Disease. Front. Neurol. *9*, 809. https://doi.org/10.3389/fneur.2018.00809.

62. Choi, I.Y., Lim, H.T., Che, Y.H., Lee, G., and Kim, Y.J. (2021). Inhibition of the Combinatorial Signaling of Transforming Growth Factor-Beta and NOTCH Promotes Myotube Formation of Human Pluripotent Stem Cell-Derived Skeletal Muscle Progenitor Cells. Cells *10*, 1649. https://doi.org/10.3390/cells10071649.

63. Yun, S.P., Kam, T.I., Panicker, N., Kim, S., Oh, Y., Park, J.S., Kwon, S.H., Park, Y.J., Karuppagounder, S.S., Park, H., et al. (2018). Block of A1 astrocyte conversion by microglia is neuroprotective in models of Parkinson's disease. Nat. Med. *24*, 931–938. https://doi.org/10.1038/s41591-018-0051-5.

64. Kim, S., Yun, S.P., Lee, S., Umanah, G.E., Bandaru, V.V.R., Yin, X., Rhee, P., Karuppagounder, S.S., Kwon, S.H., Lee, H., et al. (2018). GBA1 deficiency negatively affects physiological alpha-synuclein tetramers and related multimers. Proc. Natl. Acad. Sci. USA *115*, 798–803. https://doi.org/10.1073/pnas.1700465115.

65. Chambers, S.M., Fasano, C.A., Papapetrou, E.P., Tomishima, M., Sadelain, M., and Studer, L. (2009). Highly efficient neural conversion of human ES and iPS cells by dual inhibition of SMAD signaling. Nat. Biotechnol. *27*, 275–280. https://doi.org/10.1038/nbt.1529.

66. Polinski, N.K., Volpicelli-Daley, L.A., Sortwell, C.E., Luk, K.C., Cremades, N., Gottler, L.M., Froula, J., Duffy, M.F., Lee, V.M.Y., Martinez, T.N., and Dave, K.D. (2018). Best Practices for Generating and Using Alpha-Synuclein Pre-Formed Fibrils to Model Parkinson's Disease in Rodents. J. Parkinsons Dis. *8*, 303–322. https://doi.org/10.3233/JPD-171248.

67. Mao, X., Ou, M.T., Karuppagounder, S.S., Kam, T.I., Yin, X., Xiong, Y., Ge, P., Umanah, G.E., Brahmachari, S., Shin, J.H., et al. (2016). Pathological alpha-synuclein transmission initiated by binding lymphocyte-activation gene 3. Science *353*, aah3374. https://doi.org/10.1126/science.aah3374.

68. Kim, H., Park, J., Kang, H., Yun, S.P., Lee, Y.S., Lee, Y.I., and Lee, Y. (2020). Activation of the Akt1-CREB pathway promotes RNF146 expression to inhibit PARP1-mediated neuronal death. Sci. Signal. *13*, eaax7119. https://doi.org/10.1126/scisignal.aax7119.

69. Kim, Y.J., Lim, H., Li, Z., Oh, Y., Kovlyagina, I., Choi, I.Y., Dong, X., and Lee, G. (2014). Generation of multipotent induced neural crest by direct reprogramming of human postnatal fibroblasts with a single transcription factor. Cell Stem Cell *15*, 497–506. https://doi.org/10.1016/j.stem.2014.07.013.

70. Gavrieli, Y., Sherman, Y., and Ben-Sasson, S.A. (1992). Identification of programmed cell death in situ via specific labeling of nuclear DNA fragmentation. J. Cell Biol. *119*, 493–501. https://doi.org/10.1083/jcb.119.3.493.

71. Negoescu, A., Lorimier, P., Labat-Moleur, F., Drouet, C., Robert, C., Guillermet, C., Brambilla, C., and Brambilla, E. (1996). In situ apoptotic cell labeling by the TUNEL method: improvement and evaluation on cell preparations. J. Histochem. Cytochem. *44*, 959–968. https://doi.org/10.1177/44.9.8773561.

72. O'Brien, J., Wilson, I., Orton, T., and Pognan, F. (2000). Investigation of the Alamar Blue (resazurin) fluorescent dye for the assessment of mammalian cell cytotoxicity. Eur. J. Biochem. *267*, 5421–5426. https://doi.org/10.1046/j.1432-1327.2000.01606.x.

73. Kamiloglu, S., Sari, G., Ozdal, T., and Capanoglu, E. (2020). Guidelines for cell viability assays. Food Frontiers *1*, 332–349. https://doi.org/10.1002/fft2.44.

74. Lin, H.T., Tsai, H.Y., Liu, C.P., and Yuan, T.T.T. (2010). Comparability of bovine virus titers obtained by TCID50/ml and FAID50/ml. J. Virol. Methods *165*, 121–124. https://doi.org/10.1016/j.jviromet.2010.01.005.

75. Lee, H., Kim, E.J., Cho, I.S., Song, J.Y., Choi, J.S., Lee, J.Y., and Shin, Y.K. (2017). A serological study of severe fever with thrombocytopenia

syndrome using a virus neutralization test and competitive enzyme-linked immunosorbent assay. J. Vet. Sci. *18*, 33–38. https://doi.org/10.4142/jvs.2017.18.1.33.

76. REED, L.J., and MUENCH, H. (1938). A SIMPLE METHOD OF ESTIMATING FIFTY PER CENT ENDPOINTS12. Am. J. Epidemiol. *27*, 493–497. https://doi.org/10.1093/oxfordjournals.aje.a118408.
77. Rangan, G.K., and Tesch, G.H. (2007). Quantification of renal pathology by image analysis. Nephrology *12*, 553–558. https://doi.org/10.1111/j.1440-1797.2007.00855.x.
78. Coons, A.H., Creech, H.J., and Jones, R.N. (1941). Immunological Properties of an Antibody Containing a Fluorescent Group. Exp. Biol. Med. (Maywood). *47*, 200–202.
79. Burnette, W.N. (1981). "Western blotting": electrophoretic transfer of proteins from sodium dodecyl sulfate–polyacrylamide gels to unmodified nitrocellulose and radiographic detection with antibody and radioiodinated protein A. Anal. Biochem. *112*, 195–203. https://doi.org/10.1016/0003-2697(81)90281-5.

STAR★METHODS

KEY RESOURCES TABLE

REAGENT or RESOURCE	SOURCE	IDENTIFIER
Antibodies		
Rat monoclonal anti-D1 Dopamine Receptor	Sigma Aldrich	Cat#D6944; RRID: AB_1840807
Rabbit Polyclonal tyrosine hydroxylase (TH)	Novus Biologicals	Cat#NB300-109; RRID: AB_350437
Rabbit Recombinant Monoclonal anti-Alpha-synuclein (phospho S129) antibody	Abcam	Cat#ab168381; RRID: AB_2728613
Rabbit Recombinant Monoclonal Alpha-synuclein phospho S129 antibody	Abcam	Cat#ab51253; RRID: AB_2218489
Mouse monoclonal anti-Purified anti-α-Synuclein Phospho (Ser129)	Biolegend	Cat#825701; RRID: AB_2564891
Mouse monoclonal anti-α-Synuclein	BD Bioscience	Cat#610787; RRID: AB_398108
Rabbit Polyclonal anti-Purified anti-Tubulin beta-3 (TUBB3), neuron-specific class III beta-tubulin (TUJ1)	Biolegend	Cat#802001; RRID: AB_2564645
Chicken polyclonal anti-Microtubule-associated protein 2 (MAP2)	Invitrogen	Cat#PA1-10005; RRID: AB_1076848
Polyclonal Rabbit Anti-Glial fibrillary acidic protein (GFAP)	DAKO JAPAN	Cat#Z033429; RRID: AB_10013382
Mouse Monoclonal Anti-Glial Fibrillary Acidic Protein (GFAP) Antibody, clone GA5	EMD Millipore	Cat#MAB360; RRID: AB_11212597
Rabbit Recombinant Monoclonal Anti- ionized calcium-binding adapter molecule 1 (Iba-1)	Abcam	Cat#ab178846; RRID: AB_2636859
Rabbit polyclonal Anti-Ionized calcium binding adaptor molecule 1 (IBA1)	Wako	Cat#019–19741; RRID: AB_839504
SARS/SARS-CoV-2 Nucleocapsid Mouse Monoclonal Antibody (B46F)	Invitrogen	Cat#MA1-7404; RRID: AB_1018422
N (Nucleoprotein) Recombinant Monoclonal Antibody, FITC conjugated	Cusabio	Cat#CSB-RA33255C1GMY; RRID: AB_3083549
Polyclonal SARS-CoV-2 Nucleocapsid Antibody, Rabbit PAb, Antigen Affinity Purified	Sino Biological	Cat#40143-T62; RRID: AB_2892769
rabbit Polyclonal Anti-ACE2 antibody	Sigma Aldrich	Cat#SAB3500978; RRID: AB_3083550
Mouse Monoclonal Anti-β-Actin-Peroxidase (HRP) antibody	Sigma-Aldrich	Cat#A3854; RRID: AB_262011
Rabbit Recombinant Monoclonal SQSTM1/p62 antibody	abcam	Cat#ab109012; RRID: AB_2810880
Rabbit Polyclonal LC3A/B Antibody, Light Chain 3(LC3)	cell signaling	Cat#4108; RRID: AB_2137703
Rabbit monoclonal anti COX(cytochrome *c* oxidase) IV (3E11)	cell signaling	Cat#4850; RRID: AB_2085424
Cytochrome *c* (136F3) Rabbit mAb Antibody	cell signaling	Cat#4280; RRID: AB_10695410
Rabbit mAb Antibody HSP60 (D6F1) XP®, Heat shock protein family D (Hsp60) member 1	cell signaling	Cat#12165; RRID: AB_2636980
Rabbit Polyclonal PHB1(Prohibitin 1) Antibody	cell signaling	Cat#2426; RRID: AB_823689
Rabbit Monoclonal antibody SDHA (D6J9M) XP®, succinate dehydrogenase complex flavoprotein subunit A	cell signaling	Cat#11998; RRID: AB_2750900
Rabbit monoclonal antibody VDAC (D73D12), voltage dependent anion channel 1	cell signaling	Cat#4661; RRID: AB_10557420
Anti-SFTS (Severe Fever with Thrombocytopenia Syndrome) 10G7	Provided by Professor Yeun-Kyung Shin	Reported in the article PMID 26435543

(*Continued on next page*)

Continued

REAGENT or RESOURCE	SOURCE	IDENTIFIER
Cy™3 AffiniPure™ Polyclonal Donkey Anti-Mouse IgG (H + L)	Jackson ImmunoResearch Inc.	Cat#715-165-150; RRID: AB_2340813
Fluorescein (FITC) AffiniPure™ Polyclonal Donkey Anti-Rabbit IgG (H + L)	Jackson ImmunoResearch Inc.	Cat#711-095-152; RRID: AB_2315776
Cy™3 AffiniPure Polyclonal Donkey Anti-Rabbit IgG (H + L)	Jackson ImmunoResearch Inc.	Cat#711-165-152; RRID: AB_2307443
Fluorescein (FITC) AffiniPure Polyclonal Donkey Anti-Mouse IgG (H + L)	Jackson ImmunoResearch Inc.	Cat#715-095-151; RRID: AB_2335588
Polyclonal Goat anti-Mouse IgG-heavy and light chain Antibody HRP Conjugated	BETHYL	Cat#A90-116P; RRID: AB_67183
Peroxidase AffiniPure Polyclonal Goat Anti-Rabbit IgG (H + L)	Jackson ImmunoResearch Inc.	Cat#111-035-144; RRID: AB_2307391
Bacterial and virus strains		
SARS-CoV-2 strain BetaCoV/Korea/KCDC03/2020	Korea Disease Control and Prevention Agency (KCDC)	NCCP43326
Delta variant SARS-CoV-2 strain	Korea Disease Control and Prevention Agency (KCDC)	NCCP 43390
Severe fever with thrombocytopenia syndrome (SFTS) virus	Korea Disease Control and Prevention Agency (KCDC)	JJCB01/2021, abbreviated as CaB
Chemicals, peptides, and recombinant proteins		
Essential 8 medium	Gibco	Cat#A1517001
iMatrix-511	Matrixome	Cat#892-021
Versene solution	Gibco	Cat#15040066
Accutase	Sigma Aldrich	Cat#A6964
Geltrex™	Gibco	Cat#A1569601
(DMEM)/F12	Gibco	Cat#11320033
Minimum Essential Medium (MEM) Non-Essential Amino Acids Solution (NEAA)	Gibco	Cat#11140050
L-glutamine	Thermo Fisher Scientific	Cat#25030081
KSR medium	Thermo Fisher Scientific	Cat#10828028
N2	Gibco	Cat#17502048
Neurobasal/B27/L-glut containing medium (NB/B27	Gibco	Cat#A3653401
Poly-D-lysine	Gibco	Cat#A3890401
Laminin	Sigma Aldrich	Cat#L2020
Brain-derived neurotrophic factor (BDNF)		Cat#248-BDB-050/CF
ascorbic acid	Sigma Aldrich	Cat#A4034
glial cell line-derived neurotrophic factor (GDNF)	R&D system	Cat#212-GD-050/CF
N,2′-*O*-Dibutyryladenosine 3′,5′-cyclic monophosphate sodium salt (dbcAMP)	Calbiochem	Cat#28745
transforming growth factor, beta 3 (TGFβ3)	R&D system	Cat#243-B3-002/CF
N-[N-(3,5-Difluorophenacetyl)-L-alanyl]-S-phenylglycine *t*-butyl ester (DAPT)	Tocris	Cat#2634/10
LDN193189	STEMGENT	Cat#04-0074-02
SB431542	Tocris	Cat#04-0010-10
Recombinant mouse sonic hedgehog (SHH, C25II)	R&D system	Cat#464-SH-025/CF
purmorphamine	STEMGENT	Cat#04-0009

(*Continued on next page*)

Continued

REAGENT or RESOURCE	SOURCE	IDENTIFIER
Recombinant human/mouse fibroblast growth factor (FGF)-8b	R&D system	Cat#423-F8-025/CF
CHIR99021	STEMGENT	Cat#04-0004-02
DMEM	Gibco	Cat#11965092
Fetal bovine serum	Gibco	Cat#26140079
Penicillin–streptomycin	Gibco	Cat#15140122
Human α-Syn monomers	Proteos	Cat#RP-003
Novex™ WedgeWell™	Invitrogen	Cat#XP08165BOX
Coomassie R-250	Thermo Fisher Scientific	Cat#20278
TRIzol	Invitrogen	Cat#15596018
HiSecriptTM RH(–) RT Premix Kit	Intron Biotechnology	Cat#25087
iQ SYBR Green Supermix	Bio-Rad	Cat#1708882
TruSeq Stranded Total RNA Sample Prep Kit with Ribo-Zero H/M/R	Illumina	Cat#20040525
Terminal deoxynucleotidyl transferase dUTP nick end labeling (TUNEL)	Roche	Cat#11684795910
Tween 20	Sigma–Aldrich	Cat#TR1027-500-00
4′,6-diamidino-2-phenylindole (DAPI)		Cat#D9542-1MG
Alamar blue	Invitrogen	Cat#DAL1025
Zoletil	Virbac	Cat#212604
Rompun	Bayer	Cat#BAY1470
Optimal cutting temperature (O.C. compound)	Sakura Finetek Inc	Cat#4583
Triton	Biosesang	Cat#TR1027-500-00
Sodium azide	Sigma–Aldrich	Cat#447810250
Normal Goat serum	Jackson ImmunoResearch Laboratories	Cat#005-000-121
ABC reagents	Vector Laboratories, Inc.	Cat#PK-6101, Cat#PK-6102
SIGMAFAST 3,3-Diaminobenzidine tablets		Cat#D4293
Vector® SG Substrate Kit, Peroxidase (HRP)	Vector Laboratories	Cat#SK-4700
Halt™ Protease and Phosphatase Inhibitor Single-Use Cocktail	Thermo Scientific	Cat#1861281
Bicinchoninic Acid (BCA) Protein Assay Kit	Thermo Scientific	Cat#23225
2X Laemmli buffer	Bio-Rad	Cat#1610737
β-mercaptoethanol	Biosesang	Cat#MR1015-100-00
Nitrocellulose (NC) membranes	Bio-Rad	Cat#162-0115
Chemiluminescence (ECL)	Pierce	Cat#34580
Critical commercial assays		
Lysosomal Intracellular Activity Assay Kit	abcam	Cat#ab234622
Proteasome assay kit	Cayman chemical	Cat#10008041
AlamarBlue™ Cell Viability Reagent	Invitrogen	Cat#DAL1100
In Situ Cell Death Detection Kit, Fluorescein	Roche	Cat#11684795910
Deposited data		
Bulk RNA sequencing data	https://www.ncbi.nlm.nih.gov/geo/	Accession no. GSE211934
Experimental models: Cell lines		
H9	WiCell	Cat#WA09 (lot:WB0143)
Vero-E6 cells	ATCC	Cat#CRL-1586

(*Continued on next page*)

Continued

REAGENT or RESOURCE	SOURCE	IDENTIFIER
Experimental models: Organisms/strains		
C57BL/6N	Koatech	C57BL/6NHsd
Human angiotensin-converting enzyme 2 (hACE2) transgenic (Tg) mice	The Jackson Laboratory	Cat#JAX034860
Oligonucleotides		
Primers for qPCR	Table S6	N/A
Software and algorithms		
GraphPad Prism (version 9)	GraphPad	RRID: SCR_002798
Adobe Illustrator	Adobe	RRID: SCR_010279
Bio-Rad CFX Manager	Bio-Rad	RRID: SCR_018064
Olyvia	Olympus	RRID: SCR_016167
R software (version 4.1.0)		https://www.r-project.org/
FastQC		SCR_014583
Trimmomatic software		SCR_011848
Bowtie 2 aligner (version 2.2.5)		SCR_016368
DESeq2 software		SCR_015687
Biorender	BioRender	BioRender.com

RESOURCE AVAILABILITY

Lead contact

Further information and requests for resources and reagents should be directed to and will be fulfilled by the lead contact, Yong Jun Kim (yjkim1@khu.ac.kr).

Materials availability

The reagents used in this study are available from the lead contact with a completed Materials Transfer Agreement.

Data and code availability

- All data is provided in supplementary files.
- This paper does not report original code.
- Any further information needed to re-analyze the data reported in this paper is available from the lead contact upon request.

EXPERIMENTAL MODEL AND PARTICIPANT DETAILS

Cell line

Human ES, WA09 (H9), was purchased from WiCell (WI, USA). Human ESCs were maintained in Essential 8 medium (#A1517001, Gibco, MA, USA) on the iMatrix-511 coating material (Matrixome, Osaka, Japan) under 5% CO_2 in a humidified incubator. To avoid unintended effects of genetic mutation, hESCs only within passages 30 to 40 were collected using Versene solution (#15040066, Gibco, MA, USA) or Accutase (#A6964, Sigma Aldrich, MA, USA) and differentiated for subsequent experiments.[62] All experiments using hESCs were performed under regulation KHSIRB-20-489 approved by the institutional IRB of Kyung Hee University.[38]

Mouse model

(1) **SARS-CoV-2:** All experiments were executed at the Animal Use Biosafety Level-3 (ABL-3) facility at the Korea Zoonosis Research Institute, which is certified by the Korea Disease Control and Prevention Agency (certification number KCDC-16-3-06). The animal experiments were approved by the Institutional Animal Care and Use Committee (JBNU 2021-092), and the experimental protocols requiring biosafety were approved by the Institutional Biosafety Committee (JBNU 2021-06-003). All of the animals were kept in specific pathogen-free conditions and ventilated cages. The cages were maintained under a 12 h/12 h light/dark cycle at 24 ± 2°C with 50% ± 5% humidity. All of the mice were kept in an ABSL3 facility for stabilization and adaptation. A total of 84 human angiotensin-converting enzyme 2 (hACE2) transgenic (Tg) mice (8-week-old, male 42, female 42, JAX#034860) were purchased from The Jackson Laboratory (ME, USA) and randomly divided into three groups: **Group 1** (1) hACE Tg+PBS (n = 6; male 3, female 3), (2) hACE Tg+SARS-CoV-2 (3 days, n = 6; male 3, female 3), (3) hACE Tg+SARS-CoV-2 (10 days, n = 6; male 3, female 3); **Group 2** (1) hACE Tg+PBS (n = 6; male 3, female 3), (2) hACE

Tg+SARS-CoV-2^{WT} (n = 6; male 3, female 3), (3) hACE Tg+SARS-CoV-2^{delta} (n = 6; male 3, female 3); **Group 3** (1) sham-operated mice (sham, n = 12; male 6, female 6), (2) hACE Tg+SARS-CoV-2 (n = 12; male 6, female 6), (3) hACE Tg+Preformed fibril (hPFF) (n = 12; male 6, female 6) (4) hACE Tg+SARS-CoV-2+hPFF injected mice (n = 12; male 6, female 6).

(2) **Severe fever with thrombocytopenia syndrome virus (SFTSV):** All experiments using infectious SFTSV were conducted in an animal biosafety level 3 (ABSL-3) facility at the Animal and Plant Quarantine Agency (APQA), which is certified by the Korea Disease Control and Prevention Agency (certification number KCDC-HP-16-3-04). The animal experiments were approved by the Institutional Animal Care and Use Committee of the APQA (IACUC number 2021-569). The C57BL/6N mice were purchased from koatech (Pyeongtaek, Korea) and randomly divided into three groups: (1) PBS (n = 8; male 4, female 4), (2) SFTSV 7 days (n = 8; male 4, female 4), (3) SFTSV 30 days (n = 8; male 4, female 4).

METHOD DETAILS

DA neuron differentiation

H9 human embryonic stem cells were differentiated into DA neurons following a previously reported protocol.[63–65] The human embryonic stem cell line was disaggregated using Accutase to single cells. The cells were seeded at 1.5 × 10^6 cells per well on Geltrex (#A1569601, Gibco, MA, USA)-coated 6-well plates. Cells were grown for 11 days on Geltrex in Dulbecco's modified Eagle medium (DMEM)/F12 (#11320033, Gibco, MA, USA) with 10% KnockOut Serum Replacement (#10828010, Gibco, MA, USA), Minimum Essential Medium (MEM) Non-Essential Amino Acids Solution (NEAA) (#11140050, Gibco, MA, USA), 2 mM L-glutamine and 10 mM β-mercaptoethanol containing supplements detailed in Table S5. KSR medium was gradually shifted to N2 (#17502048, Gibco, MA, USA)-containing medium starting on Day 5 of differentiation.[63–65] The medium was changed to Neurobasal/B27/L-glut containing medium (NB/B27, #A3653401, Gibco, MA, USA) supplemented detailed in Table S5. Cells were dissociated using Accutane and replated on dishes precoated with 20 mg/mL poly-D-lysine (PDL, # A3890401 Gibco, MA, USA) and 1 mg/mL laminin (#L2020, Sigma Aldrich, MA, USA) in differentiation medium (NB/B27 with brain-derived neurotrophic factor (BDNF), ascorbic acid, glial cell line-derived neurotrophic factor (GDNF), N,2′-*O*-Dibutyryladenosine 3′,5′-cyclic monophosphate sodium salt (dbcAMP), transforming growth factor, beta 3 (TGFβ3) and N-[N-(3,5-Difluorophenacetyl)-L-alanyl]-S-phenylglycine *t*-butyl ester (DAPT).[63–65] Cells were grown with LDN193189 (100 nM, STEMGENT, MD, USA) for Days 0–11, SB431542 (10 μM, Tocris, Bristol, UK) for Days 0–5, recombinant mouse sonic hedgehog (SHH, C25II) (100 ng/mL, R&D system, MN, USA), purmorphamine (2 μM, STEMGENT, MD, USA), recombinant human/mouse fibroblast growth factor (FGF)-8b (100 ng/mL, R&D system) for Days 1–7, and CHIR99021 (CHIR; 3 mM, STEMGENT, MD, USA) for Days 3–13 in DMEM/F12 media with 10% KSR, MEM NEAA, 2 mM L-glutamine and 10 mM β-mercaptoethanol on Matrigel-coated plates. Next, the medium was gradually changed to neurobasal/B27/L-glut-containing medium (NB/B27; Invitrogen, MA, USA). Then, cells were grown with the brain-derived neurotrophic factor CHIR (BDNF, 20 ng/mL; R&D system), ascorbic acid (0.2 mM, Sigma Aldrich, MA, USA), glial cell line-derived neurotrophic factor (GDNF, 20 ng/mL; R&D system), transforming growth factor type β3 (TGFβ3, 1 ng/mL; R&D system), dibutyryl cAMP (dbcAMP, 0.5 mM; Sigma Aldrich), and DAPT (10 mM; Tocris) from Day 13 to Day 21. Differentiated cells were identified with tyrosine hydroxylase (TH, DA neuronal marker), neuron-specific class III beta-tubulin (TUJ1) (#802001, Biolegend, CA, USA), and microtubule-associated protein 2 (MAP2, neuronal marker) through western blot (Figure S1) and reverse transcriptase quantitative polymerase chain reaction (qPCR) (Table S6).

SARS-CoV-2 preparation and infection of cells

SARS-CoV-2 (NCCP43326, strain BetaCov/Korea/KCDC03/2020) was delivered by the Korea Disease Control and Prevention Agency (KCDC). For virus replication, Vero-E6 cells were infected at a multiplicity of infection (MOI) of 0.05 and cultured in DMEM (#11965092, Gibco, MA, USA) supplemented with 2% fetal bovine serum (#26140079, Gibco, MA, USA) and penicillin–streptomycin (#15140122, Gibco, MA, USA) at 37°C and 5% CO_2.[38] To infect human embryonic stem cell-derived DA neurons, 0.1 MOI/ml of virus were incubated for 1 h to allow attachment, and the infected cells were incubated after washing out the virus remaining in the medium.

Preparation of hPFFs and monomeric α-synuclein (α-syn)

Human α-Syn monomers (RP-003) were obtained from Proteos. For hPFF, Human α-Syn monomers were prepared following the Michael J. Fox Foundation's guidelines for fibril formation. α-Syn monomers were incubated in PBS at 1,000 rpm and 37°C (ATTO WSC-2630, Tokyo, Japan). After a week of incubation of the α-Syn protein, aggregates were diluted to 0.1 mg/mL with PBS and sonicated for 1 min (0.5 s pulse on/off) at 10% amplitude 3 times (SONICS & MATERIALS INC., CT, USA).[63,64,66,67]

hPFF characterization

The hPFFs were divided into nonshake, nonsonication, and sonication groups, and then characterization was performed via western blotting (Figure S1D), Coomassie blue staining (Figure S4B), transmission electron microscopy (Figure S1F). Transmission electron microscopy (TEM) images were measured using ImageJ software, data for hPFFs below 50 nm (Figure S1G). The quality of finely fragmented hPFF was confirmed through p-a-syn/TH staining (Figures S1H and S1I). Novex WedgeWell 8 to 16% gel (Invitrogen)

stained with Coomassie blue staining solution containing 0.1% Coomassie R-250 (Thermo Fisher Scientific) in 40% ethanol and 10% acetic acid for 1 h. The gel was incubated for 2 h in 10% acetic acid, 50% methanol, and 40% distilled water.

TEM OF α-SYN AGGREGATES

Human α-Syn PFF (5 μg/μL) in PBS samples were pipetted onto 200 mesh copper grids (EMS) with carbon-coated formvar film and incubated for 2 min. Excess liquid was removed by blotting. The grid was briefly placed on 10 μL of 2% uranyl acetate (w/v; Merck, Darmstadt, Germany), followed by blotting to remove excess liquid. This last step was repeated. Grids were allowed to dry before imaging on a Phillips CM 120 TEM operating at 80 kV. Images were captured and digitized with an US1000 CCD (2048 × 2048 pixel, 14 μm pixel, 100% fill factor) and 2k × 2k CCD camera (Gatan, Inc., CA, USA) by advanced microscopy techniques (Figure S1F).[68]

Reverse transcription and quantitative PCR (qPCR) analysis

Total RNA was extracted using TRIzol (Invitrogen), and the RNA concentration was measured spectrophotometrically using a Nanodrop (DeNvix Inc., NC, USA). Subsequently, 1–2 μg of total RNA was reverse transcribed to cDNA using the HiSecript RH(−) RT Premix Kit (#25087, Intron Biotechnology, Gyeonggi, Korea), and quantitative PCR was performed on the CFX Connect Real-Time PCR System using iQ SYBR Green Supermix (Bio-Rad). Relative mRNA levels were normalized to those of GAPDH for each gene. The primer sequences are listed in Table S6 appendix.

RNA sequencing and informatic analysis

Total RNA was prepared from control ($n = 2$), hPFF-treated ($n = 2$), SARS-CoV-2-infected ($n = 2$), or SARS-CoV-2-infected upon hPFF treatment ($n = 2$) samples using TRIzol. RNA quality was assessed using the Agilent 2100 Bioanalyzer (Agilent, CA, USA) and quantified using a Qubit fluorometer (Thermo Fisher Scientific, MA, USA). RNA sequencing libraries were prepared using the TruSeq Stranded Total RNA Sample Prep Kit with Ribo-Zero H/M/R (Illumina, CA, USA), and the quality of libraries was evaluated using the Bioanalyzer. Generated libraries were sequenced on an Illumina NovaSeq6000 sequencer (Illumina, CA, USA) with paired-end 150 bp reads. Quality control and preprocessing of the raw reads were performed using FastQC and Trimmomatic software. Raw reads were then mapped to the human reference genome, hg38, using Bowtie 2 aligner (version 2.2.5). Binary Alignment Map (BAM) files were then normalized using Transcripts Per Million (TPM) methods and were statistically modeled using ANOVA. Gene expression levels were quantified using featureCounts, and differential expression analysis was performed using DESeq2 software. We used a log2-fold-change cutoff of 1 and an adjusted p value cutoff of 0.05 to identify differentially expressed genes (DEGs). To visualize the overlap between the differentially expressed gene lists, we created a Venn diagram using the VennDiagram R package. All statistical analyses were conducted using R software (version 4.1.0). Validation of the differential expression results was performed using qPCR. The DEGs were further analyzed by uploading them to the DAVID web server [https://david.ncifcrf.gov, (accessed on 24 February 2022)] or KEGG Mapper [https://www.genome.jp/kegg, (accessed on 25 February 2022)].[58,69] Only genes with p values of 0.05 or less from the Gene Ontology or KEGG pathway analysis results were included in the uploaded list. RNA sequencing data generated in this study have been deposited in the Gene Expression Omnibus (GEO) database, GSE211934.

TUNEL assay for neurons

To determine cell viability, a terminal deoxynucleotidyl transferase dUTP nick end labeling (TUNEL) (#11684795 910, Roche, Switzerland) assay was performed.[70,71] The cells were washed with PBS twice, fixed with 4% buffered paraformaldehyde for 30 min and permeabilized for 5 min at room temperature. Cells were then blocked with 5% normal goat serum in PBS-0.05% Tween 20 (Sigma–Aldrich), followed by incubation with TUNEL reaction mixture (11684795910; Roche, Basel, Switzerland) for 60 min at 37°C. Nuclei were stained with 4′,6-diamidino-2-phenylindole (DAPI), and then TUNEL-positive cells were observed by using an immunofluorescence microscope (Axiovert 200 M, Zeiss, Oberkochen, Germany) according to the manufacturer's guidelines.

Alamar Blue staining

The Alamar blue assay was used to measure cell viability.[72,73] Cell culture medium was used as a control. After exposure, the suspensions were removed, and the cells were incubated with 10% Alamar blue (#DAL1100, Invitrogen, USA) for 1–4 h at 37°C. A Versamax microplate reader (Molecular Devices, CA, USA) was used to read the fluorescence at 560 nm excitation and 590 nm emission. Background values (10% Alamar blue in cell culture medium) were subtracted from each well, and the average fluorescent intensity of the triplicates was calculated to indicate cell viability.

Stereotaxic α-Syn hPFF injection

For stereotaxic injection of α-Syn hPFF, hACE2 Tg male and female mice were anesthetized with Zoletil (Virbac, Carros, France) and Rompun (Bayer, Seoul, Korea) at a ratio of 2 mg/kg tiletamine-zolazepam to 0.4 mg/kg xylazine in mice. An injection cannula (26.5 gauge) was injected stereotaxically (mediolateral, 2.0 mm from bregma; anteroposterior, 0.2 mm; dorsoventral, 2.6 mm) and unilaterally (inserted into the right hemisphere) into the STR. The infusion was performed at a rate of 0.2 μL per min, and 2 μL of α-Syn hPFF (2.5 μg/μL in PBS) or the same volume of PBS was injected into the mouse. The protocol was referenced in a previous report.[63]

SARS-CoV-2 preparation and infection of animals

Wild-type SARS-CoV-2 (NCCP43326, Wuhan-1 strain) and the Delta variant (NCCP 43390, B.1.617.2 lineage) were obtained from the National Culture Collection for Pathogens of South Korea. Thirty-eight hACE2 Tg mice of Group 1 (2) hACE2 Tg+SARS-CoV-2 (3 days), (3) hACE2 Tg+SARS-CoV-2 (10 days), Group 2 (2) hACE2 Tg+SARS-CoV-2, Group 3 (2) hACE2 Tg+SARS-CoV-2, and (4) hACE2 Tg+SARS-CoV-2+hPFF were anesthetized with Zoletil (10 mg/kg, Virbac, Carros, Frence) and then inoculated via intranasal (i.n.) inhalation with SARS-CoV-2 wild-type at a dose of $10^{3.0}$ $TCID_{50}$/mL in 1 mL DMEM. Six hACE2 Tg mice of Group 2 (3) hACE Tg+SARS-CoV-2^{delta} were anesthetized and inoculated via the i.n. inhalation of the SARS-CoV-2 Delta variant at a dose of $10^{3.0}$ $TCID_{50}$/mL. The mice were sacrificed at 3, 7, 10, and 60 days postinoculation (dpi).

Severe fever with thrombocytopenia syndrome virus (SFTSV) preparation and infection animal

Five different genotypes of human origin SFTSV (kindly provided from Korea Disease Control and Prevention Agency) and one genotype of animal-derived SFTSV (designated as JJCB01/2021, abbreviated as CaB) were used in this study. JJCB01/2021 strain was isolated from serum sample of clinically ill companion dog serum in 2021. For virus propagation, the isolates were passaged 3 times in Vero E6 cells (ATCC, VA, USA) with Dulbecco's modified Eagle's medium (DMEM) (Gibco, NY, USA) containing 2% fetal bovine serum (FBS) (Gibco, NY, USA) and 1% penicillin and streptomycin (P/S, Thermo Fisher Scientific, IL, USA) in a 37°C-incubator supplemented with 5% CO2. Cell culture supernatant was collected at 6-day post-infection (dpi) and stored at −80°C as the working virus stock for *in vivo* experiments.

The titration of SFTSV was performed as previous report.[74] Briefly, each virus was 10-fold serially diluted and inoculated to Vero E6 cells in 96-well plates. After incubation for 5–6 days at 37°C, cells were fixed by treatment with 80% acetone for 10 min. To detect cells, contain SFTSV, viral antigens were stained with a mouse monoclonal antibody to SFTSV nucleocapsid protein (against 10G7, Median).[75] Followed by FITC-conjugated anti-mouse IgG (Invitrogen, MA, USA) secondary antibody using Reed and Munch method.[76] The virus titer was determined through the 50% fluorescent assay infectious dose ($FAID_{50}$/mL) assay. The viral load of SFTSV in the mice was checked by inoculating mice with the same infectious dose (JCB01/2021, 3×10^2 $FAID_{50}$/mL) in a volume of 100 μL of PBS, respectively. The mice were monitored daily for clinical sign and survival.

Immunohistochemistry (IHC)

IHC is a technique used to visualize the localization and distribution of specific proteins or antigens within tissues or cells. The mice were transcardially perfused with heparinized 0.1 M phosphate-buffered saline (PBS). The whole brain was removed and incubated for 24 h in a fixative solution, followed by cryoprotection in 30% sucrose solution overnight at 4°C. Finally, the brains were embedded in optimal cutting temperature (O.C. compound, (Sakura Finetek Inc., CA, USA). The brain tissues were section into 40 μm-thick sections at −20°C with a cryostat machine. IHC was carried out on consecutive brain sections, selectively targeting the striatum (STRM) and ventral midbrain (VM) regions, spanning from the Olfactory bulb (OB) to the Brain stem. The frozen sections were perfused with blocking solution for 30 min at room temperature (RT) containing 0.2% Triton (Biosesang, Gyeonggi, Korea) and 0.02% sodium azide (Sigma–Aldrich) normal goat serum (Jackson ImmunoResearch Laboratories, Inc., MD, USA). The sections were incubated overnight at 4°C with primary antibodies against TH (#NB300-109, Novus Biologicals, CO, USA), glial fibrillary acidic protein (GFAP, #Z033429, DAKO JAPAN, Kyoto, Japan), and ionized calcium-binding adapter molecule 1 (Iba-1) (ab178846, Abcam). Tissues were washed with PBS and 0.1% Triton and incubated with a biotinylated secondary antibody (Vector Laboratories, CA, USA) for 1 h at RT. Sections were again washed and incubated in ABC reagents (Vector Laboratories, Inc., CA, USA), then the color reaction was developed using the SIGMAFAST 3,3-Diaminobenzidine tablets (D4293, DAB) Peroxidase Substrate Kit (Vector Laboratories) and analyzed using a BX61VS microscope (Olympus, Tokyo, Japan). Intensity graphs in the figures were generated using ImageJ software (Rasband, W.S., ImageJ, U. S. National Institutes of Health, ME, USA, http://imagej.nih.gov/ij/, 1997–2014).[77]

Immunofluorescence (IF) analysis

The first IHC study using fluorescein isothiocyanate (FITC)-labeled antibodies was conducted in 1941.[78] Immunofluorescence was performed on 30 μm-thick serial brain sections. Information for primary and secondary antibodies are described in the Key resources table. The fluorescence intensity was measured with ImageJ software. The image was opened in ImageJ and Image/Type/8-bit was selected to convert the image to grayscale. Then, Image/Adjust/Threshold was selected to set the contrast detection threshold. When the threshold window opened, the threshold level was adjusted while looking at the histogram and image. When satisfied with the threshold level, the image was converted to black and white. Next, the ROI was defined using polygon or freehand tools.[77] All images were taken using the same conditions for both control and experimental groups, and throughout the current study, we maintained consistency in analyzing all images, keeping parameters such as exposure, contrast, and brightness uniform.

Tissue and cell lysate preparation

To separate the soluble and insoluble fractions of Triton X-100 from DA neurons or tissues, they were harvested and processed into nonionic detergent (soluble and insoluble) fractions in lysis buffer containing PBS, 1% Triton X-100, Halt Protease and Phosphatase Inhibitor Single-Use Cocktail (100X) (#1861281, Thermo Scientific). The lysates were centrifuged at 15,000 ×*g* for 20 min at 4°C. The resulting supernatant (soluble) fractions were collected. The pellet was washed in PBS three times and solubilized in lysis buffer containing 1% SDS and 0.5% sodium deoxycholate. The samples were centrifuged, and the resulting supernatants (insoluble) were collected. The total protein concentration was determined using the Pierce Bicinchoninic Acid (BCA) Protein Assay Kit (#23225,

Thermo Scientific) with bovine serum albumin (BSA) standards. The concentrations of the samples were equalized to 20 μg. Samples were mixed with 2X Laemmli buffer (Bio-Rad, CA, USA) supplemented with β-mercaptoethanol (Bio-Rad) and boiled for 5 min at 95°C.

Western blot analysis

Western blotting is a widely used technique for protein detection and quantification.[79] The loading protein concentration was 20 μg/mL. Proteins were separated by sodium dodecyl sulfate–polyacrylamide gel electrophoresis (SDS–PAGE) and transferred onto nitrocellulose (NC) membranes (0.45 μm, #162-0115, Bio-Rad) for immunoblotting. Immunoblotting was performed with the indicated antibodies, and immunoblot bands were visualized with chemiluminescence (Pierce, IL, USA) and photographed using the ChemiDoc image system (Bio-Rad). Densitometric analysis of the bands was performed using ImageJ software.

Lysosomal intracellular activity assay

The assessment of lysosomal activity measured with a self-quenched substrate, following the protocol provided by the manufacturer (Lysosomal Intracellular Activity Assay kit, Abcam, Cambridge, United Kingdom; Catalog No. ab234622). Briefly, the DA neurons were exposed to the self-quenched substrate for 1 h at 37°C. Subsequently, the cells underwent a rinse with the cold assay buffer supplied in the kit. The treated cells were then fixed using 4% paraformaldehyde for 15 min and permeabilized with 0.1% Triton X-100 for 30 min. Finally, the specimens were mounted with media containing DAPI and examined using a confocal fluorescence microscope (AX/AXR, Nikon, Japan).

20S Proteasome activity

The determination of 20S Proteasome activity in lysates obtained from DA neurons exposed to SARS-CoV-2 or/and hPFF was conducted using the 20S Proteasome Assay Kit (#10008041; Cayman chemical), following the protocol provided by the manufacturer. In summary, a synthetic 20S substrate, SUC-LLVY-AMC, was used. Upon cleavage by the active enzyme, this substrate produces a highly fluorescent product, which was quantified using excitation and emission wavelengths of 365 nm and 495 nm, respectively.

QUANTIFICATION AND STATISTICAL ANALYSIS

All data were analyzed using GraphPad Prism 7.0 software. Data are presented as the mean ± standard error of the mean (S.E.M.) or mean ± standard deviation (S.D.) with at least three biologically independent experiments. Representative images are obtained from at least three biologically independent experiments. Unpaired two-tailed Student's t tests or one-way ANOVAs followed by Tukey's multiple comparisons test were used to assess statistical significance. $p < 0.05$ was considered significant.